Multi-Site Non-Methane Hydrocarbon Source Apportionment and Ozone Insights in Southern Taiwan Using Positive Matrix Factorization

Duy-Hieu Nguyen[1], Hsin-Cheng Hsieh[1], Mao-Chang Liang[2], Neng-Huei Lin[3], Chieh-Heng Wang[4**], Jia-Lin Wang[1*]

[1] Department of Chemistry, National Central University, Taoyuan, 320317, Taiwan

[2] Institute of Earth Sciences, Academia Sinica, Taipei 115201, Taiwan

[3] Department of Atmospheric Science, National Central University, Taoyuan, 320317, Taiwan

[4] Center for Environmental Studies, National Central University, Taoyuan, 320317, Taiwan

Correspondence to:

[*]Jia-Lin Wang (cwang@cc.ncu.edu.tw)

[**] Chieh-Heng Wang (chwang1110@gmail.com)

Abstract

Ozone pollution remains a persistent challenge in Taiwan's Kaoping region due to dense industrial and urban emissions. Using high-resolution, hourly observations from three Photochemical Assessment Monitoring Stations (PAMS) combined with Positive Matrix Factorization (PMF), this study resolved eight distinct sources of non-methane hydrocarbons (NMHCs), key precursors of ozone formation. The time-resolved PMF output captured source-specific temporal patterns—as shown by the acetylene factor at Linyuan (R^2 = 0.99 with observations)—providing an intrinsic check on model performance and facilitating spatial interpretation of sources. Petroleum-related emissions dominate NMHC mass at all sites but are more prominent at Xiaogang, while aged air masses substantially enhance ozone pollution at downwind locations such as Linyuan and Chaozhou, underscoring the role of regional transport and atmospheric aging. Although mixed sources from vehicular and solvent emissions contributed less mass, they dominated ozone formation potential (OFP) due to higher chemical reactivity. Notably, their influence persisted even under moderate ozone conditions, indicative of a VOC-limited regime. Overall, these results emphasize that effective ozone mitigation in southern Taiwan requires coordinated control of petroleum, mobile, and solvent emissions, and demonstrate the value of multi-site, year-round, high-time-resolution NMHC measurements for constraining ozone precursors.

1 Introduction

Volatile organic compounds (VOCs) are key precursors in atmospheric chemistry and play a substantial role in determining air quality (Guan et al., 2020; Guo et al., 2017; Finlayson-Pitts and Pitts Jr, 1993). In the presence of nitrogen oxides (NO_x) and sunlight, VOCs undergo photochemical reactions that lead to the formation of ground-level ozone (O_3), while their oxidation products contribute to secondary organic aerosol formation (Wu et al., 2024; Mcfiggans et al., 2019). These processes are particularly intensified in rapidly industrializing and urbanizing regions, where elevated emissions and complex atmospheric interactions amplify air pollution (Zhang et al., 2022). The resulting decline in air quality poses substantial risks to both human health and ecosystems (Ramírez et al., 2019; Xu et al., 2022). Given their complex roles and diverse emission sources, a detailed characterization of ambient VOCs is essential to advance our understanding of their source origins, chemical behavior, and contributions to air pollution.

The impact of VOCs on ozone formation critically depends on the local chemical regime—whether ozone production is VOC-limited or NO_x-limited (Kleinman et al., 2002; Sillman, 1999). In VOC-limited environments, common in densely industrialized and urbanized areas, ozone levels are more responsive to changes in reactive VOC concentrations, whereas in NO_x-limited conditions, ozone formation is constrained by nitrogen oxide availability. Several studies in East and Southeast Asia have emphasized this spatial heterogeneity of ozone sensitivity (Li et al., 2019; Wang et al., 2021; Ren and Xie, 2022). In Taiwan, both modeling and observational evidence indicate that southern and western regions typically exhibit VOC-limited or transition regimes, while rural and downwind areas are more NO_x-limited (Chang et al., 2022; Chen et al., 2021b). This regime dependence underscores the need for region-specific precursor management and highlights the importance of identifying the dominant reactive VOC sources that most effectively drive ozone formation. Understanding these sensitivities provides an essential framework for interpreting ozone formation potential (OFP) derived from NMHC source contributions.

Traditional VOC source analysis often relies on passive sampling techniques, such as using canisters at strategic locations to capture spatial and temporal variations in ambient concentrations (Dumanoglu et al., 2014; Mo et al., 2015; Wang et al., 2018; Dong et al., 2024). While effective for regional assessments, these methods lack the high temporal resolution required for detailed source apportionment. To overcome this limitation, automated gas chromatograph (auto-GC) systems have been developed, offering continuous, high-frequency VOC measurements that better support the analysis of dynamic emission patterns (Wernis et al., 2022; Su et al., 2016; Chen et al., 2014; Henry, 2013). In Taiwan, the Environmental Protection Administration (EPA) has established a Photochemical Assessment Monitoring Stations (PAMS) network to provide real-time NMHCs monitoring data—a subset of VOCs—forming a technical foundation for evidence-based air quality management and research. These sophisticated monitoring techniques form a foundation for detailed source apportionment studies (Chen et al., 2021a; Gu et al., 2020; Languille et al., 2020), enabling more accurate evaluation of emission contributions and their temporal variations. Initially, this network lacked a standardized approach for identifying specific NMHC sources, with only one of the nine stations incorporating targeted source-tracking capabilities in 2007 (Chen et al., 2014). However, since 2013, the network has expanded to track emissions from major industrial zones, growing to a total of 15 stations to better support the EPA's regulatory and scientific objectives (Nguyen et al., 2025).

The Kaoping region, located in southern Taiwan, is home to one of the country's largest industrial complexes, situated near Kaohsiung Port—an important maritime trade hub in East Asia (Yeh et al., 2022). This region faces persistent air quality challenges due to intensive industrial activity, including petrochemical manufacturing, steel production, and power generation, which collectively represent dominant sources of anthropogenic NMHC emissions (Huang and Hsieh, 2019). In addition to the industrial activities, multiple emission sources — including vehicular traffic, ships in ports, urban development, biogenic activity, and long-range transport of pollutants further burden the area's air quality (Chou et al., 2022; Lin et al., 2007). Vehicular emissions, particularly those associated with gasoline combustion and fuel evaporation, are recognized as significant contributors to ambient NMHC levels in

urbanized environments. These sources are commonly characterized by elevated concentrations of light alkanes and related gasoline-associated species (Shao et al., 2016; Mo et al., 2017). At the same time, the presence of isoprene from vegetation and meteorological processes—such as sea-land breeze circulations and seasonal monsoons—complicates the chemical transformation and transport of NMHCs across the region (Li and Wang, 2012; Cheng et al., 2016). The local EPA authority has implemented emission control strategies targeting major industrial zones to address these environmental concerns. These measures include stricter emission standards, technical support for pollution reduction, and mandatory installation of factory gas recovery and treatment systems. Despite these efforts, residents adjacent to industrial parks continue to express concerns about air quality issues (Ko, 1996; Deng et al., 2022), suggesting that current measures have not fully mitigated the impact of VOC emissions on surrounding communities. Given these complex and intertwined emission sources, high-resolution NMHC monitoring from the PAMS network in the Kaoping region offers a valuable database for investigating source contributions and understanding their influence on regional air quality to improve air pollution management and air quality.

To quantitatively determine the contribution of different emission sources, receptor models such as Chemical Mass Balance (CMB) and PMF are widely applied in atmospheric research (Su et al., 2019; Na and Kim, 2007; Liu et al., 2008b; Lingwall and Christensen, 2007). Each approach has its strengths and limitations. CMB requires detailed and well-characterized source profiles and is sensitive to collinearity among input species, which can limit its applicability in complex source environments. In contrast, PMF is a data-driven technique that extracts source profiles and their contributions directly from ambient measurements, making it more flexible in situations where comprehensive source profiles are unavailable but depend on a sufficiently large and high-quality dataset (Su et al., 2016). Recent advances allow PMF to incorporate auxiliary information (e.g., known marker species or source profiles), improving source identification accuracy (Yang et al., 2022). In this context, the continuous, speciated NMHC data provided by the PAMS network create an ideal foundation for applying PMF to source apportionment in the Kaoping region, where emission sources are diverse. However, identifying sources is only one part of the broader picture of air quality. To fully understand pollution dynamics in this region, it is also essential to consider meteorological factors that influence the dispersion, accumulation, and transport of NMHCs.

To address this, many studies have coupled PMF with the Conditional Probability Function (CPF), which integrates PMF-resolved source contributions with wind direction data to infer the likely directions of pollution sources (Pekney et al., 2006; Zhou et al., 2018; Pallavi and Sinha, 2019). CPF analyses typically rely on the time series of factor contributions generated by PMF to calculate conditional probabilities of wind directions associated with elevated contributions (e.g., using the 75th percentile threshold). While CPF enhances the spatial interpretation of PMF outputs, it primarily focuses on wind direction patterns and does not fully exploit the rich temporal variability captured in the PMF-resolved factor time series. Consequently, these temporal features are rarely used to further investigate source behavior, even though they contain valuable information, such as peak events, seasonal trends, or

episodic spikes in individual sources. Importantly, high-contribution events in specific time windows provide an opportunity to integrate PMF with air mass back-trajectory analysis, linking these peaks to possible upwind source regions. This approach enhances the interpretability of PMF beyond statistical association and opens new avenues for spatiotemporal source identification.

In Taiwan, PMF has been widely applied to support evidence-based air-quality policymaking; however, most studies have concentrated on northern (Kuo et al., 2014; Liao et al., 2017; Liao et al., 2024) and central regions (Su et al., 2019). Applications of CPF in conjunction with PMF have also been largely limited to central Taiwan (Huang and Hsieh, 2019; Chen et al., 2019), leaving the Kaoping region comparatively understudied—particularly in terms of combining PMF, CPF, and trajectory analyses to identify industrial and transported NMHC sources. Thus, this study aims to bridge this gap by applying PMF and CPF to identify and characterize NMHC sources in the Kaoping region and analyze the temporal features of PMF factor contributions to guide trajectory-based source tracking. By identifying high-contribution episodes for source factor and performing back-trajectory analyses during those episodes, we can confidently infer the likely geographic origins of the emissions. In addition, the OFP associated with each source was estimated to evaluate its relative impact on ozone production. Compared to most PMF studies that rely on data from a single receptor site and limited time resolution, our study leverages three PAMS sites with year-round hourly data and distinct source–receptor characteristics, allowing for a more robust source apportionment and regional representation. This multi-PAMS framework offers insights into NMHC dynamic emissions and transport in one of the most industrialized areas in Southern Taiwan.

2 Methodology

2.1 Study site description

This study focuses on source apportionment of ambient NMHCs in the highly industrialized Kaoping region of southern Taiwan, approximately one-third the size of the New York metropolitan region, based on measurements from three PAMS monitoring sites: Xiaogang, Linyuan, and Chaozhou. The distinct locations of three sites and environmental settings provide a comprehensive view of source–receptor relationships across the region. Xiaogang, located in southern Kaohsiung, is a mixed urban-industrial area heavily influenced by emissions from multiple industrial activities. These include large petrochemical complexes, a regional airport, steel mills, metallurgical processing plants, shipyards, and power stations. In addition, maritime operations from Kaohsiung Harbor—one of the busiest ports in Asia—contribute significantly to local NMHC levels. Linyuan, situated along the southwestern coast and downwind of Kaohsiung's industrial corridor, is situated next to a large petrochemical complex frequently receiving high-concentration plumes from nearby facilities under the influence of coastal meteorology. Chaozhou, by contrast, is more inland and characterized by agricultural and vegetative land use, with minimal influence from industrial and urban anthropogenic sources. However, due to its geographic position downwind of the Kaohsiung industrial corridor, Chaozhou is susceptible to the regional pollution transported from neighboring urban and industrialized areas. As such, it serves as a receptor site for background air quality conditions with intermittent influence from upwind

anthropogenic emissions. Together, the three sites offer spatial and environmental contrasts that support robust source apportionment and allow for evaluation of both local emission characteristics and regional transport dynamics in the Kaoping region.

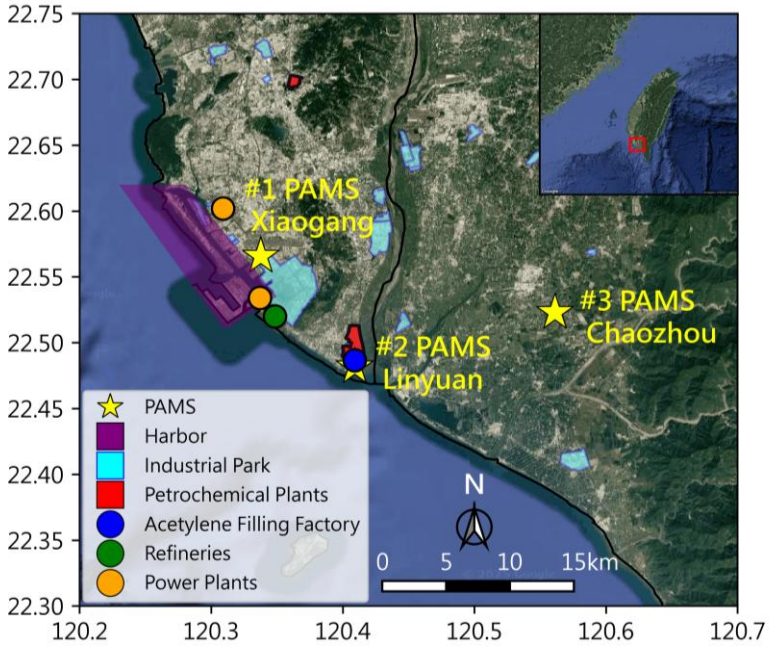

Figure 1: Study region with marked industrial facilities. Base map from Google Maps (Map data ©2025 Google)

2.2 Data collection

All three sites are equipped with PAMS, enabling high-temporal-resolution measurements of speciated NMHCs (Fig. S1). Each station employs an automated gas chromatograph system (Clarus 500 GC, PerkinElmer), configured with dual flame ionization detectors (FIDs) and thermal desorption units (TM-TD1, PerkinElmer). This TD-GC/FID setup allows for hourly quantification of 54 NMHC species ranging from C_2–C_{11}. Ambient air is sampled at a flow rate of 15 mL/min over 40 minutes, yielding approximately 600 mL of air per sample, and then passes through a Nafion dryer (500 sccm counter-flow) to eliminate excess humidity during sample collection. No ozone scrubber is needed, as the system features short, inert-coated sampling tubing, effectively minimizing the likelihood of ozone reactions. Samples are pre-concentrated at –30 °C and desorbed at 325°C for GC injection. A two-column separation strategy with a Deans switch is implemented to improve chromatographic resolution. Following desorption, analytes are first transferred to the BP-1 column. The Deans switch is then route lighter hydrocarbons (C_2–C_5) from the BP1 column to an Al_2O_3 PLOT column (50 m × 0.32 mm i.d., 5.0 µm, Varian), while heavier compounds (C_6–C_{11}) are directed through an uncoated column. Instrument calibration is conducted every three days using certified standard gas mixtures containing the 54 target species (Spectra Gases, Branchburg, USA), ensuring data quality with a measurement precision (1σ) maintained below 4%.

In addition to VOC measurements, this study incorporates hourly ancillary data from the Taiwan Air Quality Monitoring Network (TAQMN), including O_3 and meteorological parameters such as wind

speed and wind direction. This integrated dataset supports a comprehensive analysis of photochemical activity, emission dynamics, and pollutant transport mechanisms across the three monitoring environments: urban-industrial-port (Xiaogang), coastal-industrial (Linyuan), and inland-rural (Chaozhou). Data cleaning was performed prior to analysis to ensure consistency across datasets. TAQMN measurements were first screened to remove invalid entries, including missing values, instrument flags, any non-numeric values associated with routine maintenance, calibration events, power outages, or temporary instrument shutdowns. After this quality-control procedure, the TAQMN 2024 dataset achieves approximately 98% data coverage across the three sites.

2.3 NMHC source apportionment model

PMF is a receptor-based modeling technique widely used for identifying and quantifying contributions of pollution sources to ambient air quality. Originally developed by Paatero and Tapper (1994) and refined in subsequent work (Paatero, 1997), PMF has been extensively applied to NMHCs source apportionment in various urban and industrial environments (Guo et al., 2011; Zhang et al., 2015). The method decomposes the observed concentration matrix (X) into two non-negative matrices: the source contribution matrix (G) and the source profile matrix (F), along with a residual matrix (E). The model accounts for measurement uncertainty and identifies latent factors representing individual sources, each characterized by a distinct chemical profile and temporal pattern. Detailed mathematical formulations are described in prior studies (Su et al., 2019; Han et al., 2023; Huang and Hsieh, 2019).

In this study, we applied the U.S. EPA's PMF 5.0 software to perform source apportionment of NMHCs measured at the three PAMS sites in the Kaoping region. The input to the model consisted of concentration and uncertainty matrices constructed from hourly NMHC measurements. Uncertainty (Uij) was calculated based on species concentrations (Xij) and minimum detection limits (MDL) as follows:

$$U_{ij} = \sqrt{\left(0.5 \times MDL_j\right)^2 + \left(error\ fraction \times X_{ij}\right)^2} \quad (1)$$

For concentrations below MDL, the value was substituted with half MDL with uncertainty set at $\frac{5}{6}$ MDL, and an error fraction (10%). Missing values were excluded from the input dataset to maintain model reliability. To ensure a consistent and robust dataset across the three sites and four seasons, species selection was based on signal-to-noise (S/N) ratios and detection frequency following EPA PMF guidance. Specifically, species with S/N ratios < 0.1 or missing data with occurrences more than 4 instances were classified as "bad" and excluded, while those with 0.1 ≤ S/N < 2 were down-weighted as weak species. This screening process resulted in a final set of 22 out of the 54 species that were consistently detectable and quantitatively reliable across all sites and seasons (Table S1). Model stability was then evaluated through multiple diagnostic procedures. First, factor numbers from 3 to 8 were tested, each with 100 independent runs using random seed initialization. The optimal number of factors was selected based on $Q_{(robust)}/Q_{(true)}$ values that were close to 1.0, reproducibility of factor profiles across runs assessed via Bootstrap (BS) analyses (>95% matching), and the interpretability and physical plausibility of the resulting source profiles. Together, these procedures confirm that the PMF solution provides a robust and well-constrained representation of NMHC sources in the study region, while the consistent selection of 22 species ensures comparability across all seasonal and site-specific analyses.

2.4 Directional analysis with CPF and trajectory modeling

The CPF was employed to identify the likely directional origins of pollution sources by analyzing the relationship between elevated PMF factor timeseries contributions and wind direction. First, source contribution timeseries obtained from PMF output were used, with each factor representing a distinct emission source (e.g., petrochemical, solvent usage, aged air mass). Wind speed and wind direction data were integrated with PMF output to determine directional influence.

$$CPF_{\Delta\theta} = {}^{n_{\Delta\theta}}/_{m_{\Delta\theta}} \quad (2)$$

CPF was computed as the ratio of the number of times the factor contributions exceeded the threshold within a given wind sector ($n_{\Delta\theta}$) to the total number of valid observations in that sector ($m_{\Delta\theta}$). Wind direction was divided into 16 equal intervals (22.5° per sector) to ensure robust analysis. For each PMF-resolved factor, the 70th percentile was the threshold to isolate the plume events, as it effectively filtered out moderate events while retaining sufficient data for statistically stable and interpretable CPF results (Table S2). Higher CPF values in specific wind sectors indicated stronger contributions from sources in that direction. CPF plots were generated for each PMF factor to visualize dominant source directions and assess consistency with known emission source locations, meteorological patterns, and local topography.

Our developed trigger back-trajectory is employed to further utilize the time series features from PMF factor contribution, particularly their episodic spikes or peak events. Unlike traditional Lagrangian models such as HYSPLIT, which simulate long-range air mass transport using synoptic meteorological fields, the trigger back-trajectory model is optimized for short-range, near-surface pollution episodes using high-resolution wind observations from receptor sites. Each trajectory is then visualized and mapped using GIS tools layered onto spatial imagery via the Google Maps API. By aggregating multiple trajectories associated with similar high-concentration events, a trajectory ensemble analysis is conducted to identify convergence zones, which are likely source regions. This hybrid approach improves the spatial interpretability of PMF results by complementing factor profiles and CPF with spatiotemporal back-tracing, providing a robust framework for identifying not just what the sources are, but when and where they likely originated.

2.5 Ozone formation potential and uncertainty consideration

The OFP of each NMHC species was estimated using the Maximum Incremental Reactivity (MIR) coefficients developed by (Carter, 2010). The OFP for compound *i* was calculated as:

$$OFP_i = C_i \times MIR_i \quad (3)$$

Where C_i (ppb) is the measured mixing ratio of the species, and MIR_i (g O_3 g^{-1} VOC) is its reactivity coefficient (Table S1). The MIR scale represents ozone yield under low VOC/NO_x (i.e., high-NO_x or VOC-limited) conditions, where ozone formation is primarily sensitive to changes in VOC abundance. This assumption aligns with previous photochemical studies indicating that ozone formation in southern Taiwan is predominantly VOC-limited (Chang et al., 2022).

The uncertainty associated with OFP estimation was inherently accounted for during the PMF analysis. These uncertainties were used to construct the PMF input uncertainty matrix, which determines the weighting of each data point in the model fitting. As the OFP was calculated from the PMF-resolved

factor contribution time series, the measurement uncertainties are inherently reflected in the factor contributions. While this approach propagates measurement uncertainty into OFP estimates, it is important to note that OFP represents a photochemical potential, not realized ozone formation, and does not capture the nonlinear interactions that govern actual ozone production.

3 Results and discussion

3.1 PAMS data overview

Leveraging three PAMS sites in a region with heavy industrial loading, this study captures the spatial variability of source dynamics, providing a clearer picture of how NMHC levels are shaped. The annual mean concentrations of NMHC—calculated from 54 species—exhibited pronounced spatial heterogeneity across the sampling sites. As illustrated in Fig. 2a, the level varied considerably, with Linyuan recorded the highest average concentration (28.20 ± 37.28 ppb), followed by Xiaogang (18.90 ± 11.85 ppb) and Chaozhou (9.88 ± 6.92 ppb). However, the corresponding median values (10.92, 13.68, and 6.92 ppb, respectively) indicate that these distributions are skewed, particularly at Linyuan, where the mean is substantially higher than the median, reflecting occasional extreme emission events likely driven by dense petrochemical operations. Meanwhile, Xiaogang, with a mean slightly higher than its median, represents a mixed urban-industrial setting, where both vehicular emissions and industrial activities contribute to ambient NMHC levels. In contrast, Chaozhou exhibits lower mean and median concentrations, characteristic of a predominantly agricultural environment. Notably, an anomalous elevation was observed in Chaozhou during August, and this feature will be further examined in later sections. Statistical analysis reveals that, after removing the elevated window, the extreme short-duration did not alter the central tendency of the observations, with minimal impact observed on the statistical metrics (Table S3). A comparative analysis indicates that NMHC concentrations in this study were generally lower than those reported in Guangzhou (42.74 ppb), Wuhan (34.65 ppb), Chengdu (41.8 ppb), and Beijing (29.12 ppb), which were selected due to their similar urban environments (Li et al., 2022; Hui et al., 2018; Zou et al., 2015; Song et al., 2018). The difference reflects the effectiveness of emission control measures in Taiwan, supported by stringent regulations, cleaner fuels, and strengthened industrial emission standards (Moe, 2022, 2023). Additionally, meteorological factors, such as higher wind speeds at Xiaogang and Chaozhou, likely contribute to dilution and dispersion, further shaping the observed NMHC distribution. The combined consideration of mean and median reveals both typical ambient levels and the influence of short-term emission peaks in understanding NMHC exposure across the region.

3.2 NMHC compositions

While NMHC concentrations provide a broad picture of emission intensities, a more detailed understanding of their pollution requires an analysis of their chemical composition. The NMHC profiles at Chaozhou, Linyuan, and Xiaogang exhibited distinct characteristics, reflecting their diverse emission sources and atmospheric processing (Fig. 2b). Across all sites, 54 NMHC species were quantified and categorized into five major groups: alkanes, alkenes, aromatics, alkynes (ethyne) and isoprene.

Alkanes dominated the NMHC composition at Chaozhou and Xiaogang, comprising 61% and 64% of total NMHC, respectively, while accounting for only 36% at Linyuan. This alkane dominance is

consistent with previous findings in Asian cities (Zhang et al., 2020; Song et al., 2020), reflecting their long atmospheric lifetimes and broad emission sources, including hydrocarbon processing and gasoline-related activities. Ethane, propane, n-butane and isobutane alone contributed about 42% of the total concentration across three sites, with enhanced levels of n-butane and isobutane particularly evident at Xiaogang and Chaozhou. In contrast, Linyuan exhibited a distinctly different chemical profile, with ethyne (acetylene) making up 38% of its total NMHCs, substantially higher than at Chaozhou (14%) and Xiaogang (3%). This substantial presence of acetylene indicates localized, intense anthropogenic activities. Notably, Linyuan recorded the highest annual mean NMHCs. However, this ranking is primarily driven by its elevated acetylene levels. When acetylene is excluded, the relative ranking changes, and Linyuan shifts to second place after Xiaogang (Fig. S2), highlighting the disproportionate influence of a single pollutant species on the site's total NMHC burden.

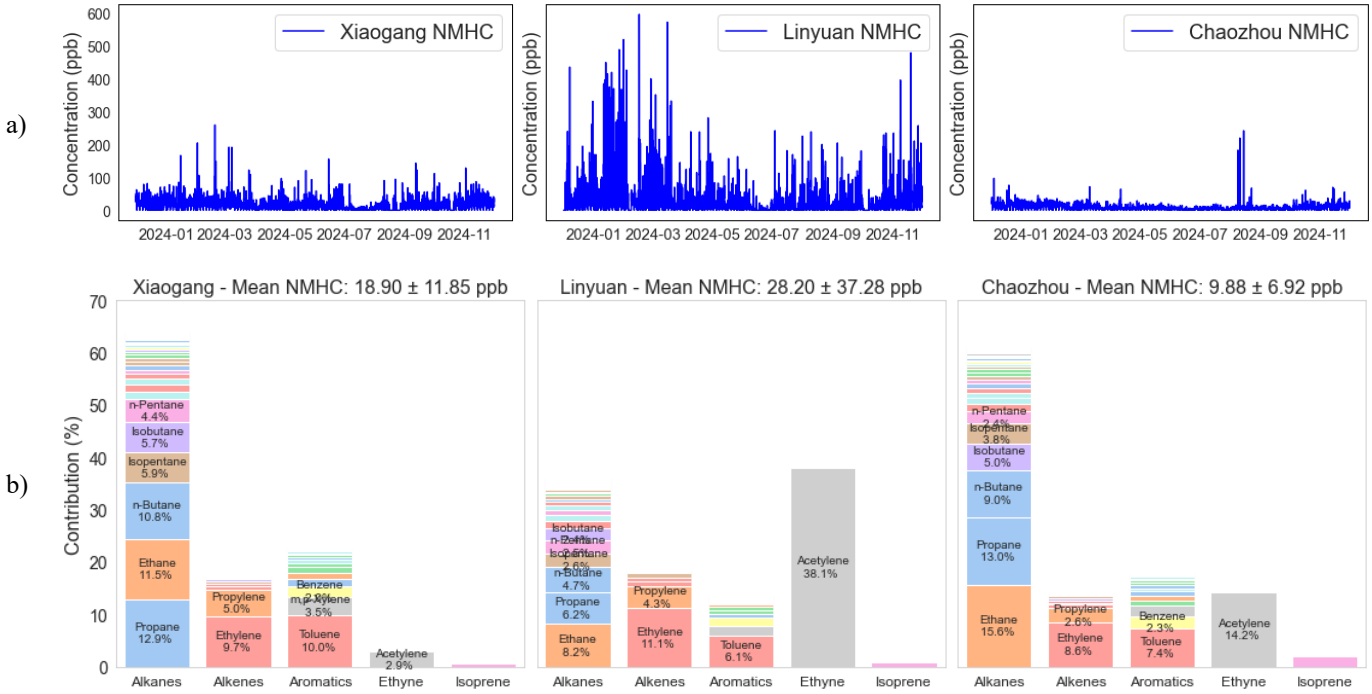

Figure 2: Time series of total NMHC concentrations and mean composition of NMHC groups at Chaozhou, Linyuan, and Xiaogang in 2024. (a) Hourly variations illustrate temporal patterns and notable episodic peaks at each site. (b) Mean NMHC concentrations (ppb) and percentage contributions of individual compounds within major chemical groups. The mean concentrations of individual species are presented in Fig. S3.

Aromatic compounds formed the second-largest group at Xiaogang (22%), followed by Chaozhou (17%) and Linyuan (13%). The predominance of toluene and m,p-xylene across all sites aligns with findings from previous studies in Shanghai (Zhang et al., 2018) and Xi'an (Song et al., 2020), indicating contributions from solvent use, paint application, and industrial processes. The notably higher toluene proportion at Xiaogang suggests significant emissions from solvent-related industries, such as coating and painting. Alkenes accounted for a relatively stable fraction across sites (approximately 14% at Chaozhou, 18% at Linyuan and Xiaogang), with ethylene being the dominant species. Given that ethylene is primarily emitted from combustion and petrochemical activities, its consistent presence underscores the role of anthropogenic sources in shaping the NMHC composition.

These pronounced differences in NMHC chemical profiles highlight the spatial heterogeneity of emission sources and atmospheric processes across the study area. The alkane-rich profiles of Chaozhou and Xiaogang contrast sharply with the ethyne-dominated composition at Linyuan, illustrating how industrial activities significantly influence ambient NMHC signatures. Understanding these chemical distinctions is crucial for designing targeted pollution control strategies tailored to the unique emission characteristics of each urban environment.

3.3 Resolved Source profiles

As mentioned before, some measured NMHCs were excluded from PMF analysis due to their greater volume of data below MDLs. Consequently, the numbers of NMHC species input into the model for source apportionment were 22 species, accounting for 88.9%, 91.7%, and 93.8% of the full 54 NMHCs concentration at Xiaogang, Linyuan, and Chaozhou, respectively. Based on the model used, there were eight distinct sources of resolved factors (Figs. 3, 5, and S4) which are petrochemical I (Petro I), petrochemical II (Petro II), refinery, industrial fugitive emissions, mixed sources (Mixed), photochemical aged (Aged air mass), acetylene, and biogenic. Consistent source profiles were observed across seasons and at all three monitoring sites, underscoring the robustness of the PMF results and confirming the dominant contribution of specific source factors throughout the study area (Fig. 3).

3.3.1 Common sources

a) Petrochemical factors

The PMF analysis revealed a strong presence of ethylene and propylene, both of which are key raw materials in the petrochemical industry (Leuchner and Rappenglück, 2010). Ethylene is the most important feedstock in the synthetic organic chemical manufacturing industry, serving as a building block for a wide array of chemicals for making plastics, antifreeze solutions, and solvents. Similarly, propylene is a critical precursor in producing various petrochemical products. Our results are in agreement with those of Xie and Berkowitz (2006), who reported that ethylene and propylene were the main NMHCs emitted from petrochemical emissions. The factor represented by a single dominant compound of ethylene and propylene can be referred to here as the Petro-I and II (Fig. 3). Ethylene and propylene did not appear in proportion despite their shared industrial origin due to the spatial heterogeneity in emission sources across the large campus of the petro-complex at the studied sites. Notably, in summer, the Petro-I profile becomes especially pronounced at Xiaogang, characterized by increased ethane and propane as by-products of cracking operations (Thiruvenkataswamy et al., 2016; Pedrozo et al., 2020). They are prone to fugitive emissions or evaporative losses, particularly from storage tanks at elevated temperatures.

The PMF-resolved time series contribution for Petro-I and Petro-II reveals episodic spikes, with no clear pattern of increase or decrease during weekends (Fig. S5), suggesting these events may be associated with perennial petrochemical processes with constant fugitive emissions. Linyuan consistently exhibits the highest contributions for both Petro-I and II during winter and, to a lesser extent, spring and fall, followed by a distinct decline in summer. In contrast, Xiaogang's Petro-I contributions rise notably in fall and remain elevated into the winter with a lesser extent in spring, though Petro-II activity there is less pronounced. Chaozhou records consistently low contributions for both factors throughout all seasons,

indicating minimal influence from these industrial sources (Fig. S5, green line). Spatial analysis of the preferred source directions for Petro-I and II further underscores site-specific differences. At Xiaogang, the dominant influence comes from northerly winds in fall, spring, and winter (Fig. 4, red line), while stronger southerly winds are observed in summer and peak in fall, emphasizing the role of prevailing winds in the Kaohsiung area. It highlights the complexity of source contributions and the importance of meteorological conditions in modulating observed concentrations. This pattern aligns with the spatial distribution of active petrochemical facilities in Kaohsiung City, as shown in Fig. 1, and is reflected in the dominant source directions in Fig. 4. For Linyuan, the prevailing source direction is from the northwest, consistent with the site location downwind of Linyuan industrial areas (Fig. 4, orange line).

b) Refinery factor

The refinery-related emissions were primarily composed of C3–C5 alkanes, including propane, isobutane, n-butane, isopentane, and n-pentane (Fig. 3). While n-pentane is commonly identified as a tracer of gasoline evaporation in VOC source profiles, and n-butane is also abundant in fuel vapors (Kumar et al., 2020), they are also associated with emissions from petroleum refining processes (Wei et al., 2016). The separation of refinery and petrochemical sources in PMF analyses has also been documented in previous studies (Kim et al., 2005; Buzcu and Fraser, 2006; Dumanoglu et al., 2014; Chen et al., 2019) and in CMB modeling (Scheff et al., 1989). The PMF-resolved time series contributions are relatively stable and exhibit consistent patterns across most sites and seasons, except for a notable increase at Xiaogang during summer (Fig. S5). Occasional peaks in the PMF-resolved time series at Xiaogang and Linyuan suggest the presence of episodic events or localized influences, likely associated with butanes, which are the most dominant contributors to this factor. Yet, there is no clear indication of a long-term trend or significant weekend effect, highlighting the ongoing and process-driven nature of refinery emissions. Chaozhou consistently registers the lowest refinery factor contributions in all seasons, likely due to its inland downwind position and limited proximity to major refinery facilities. Directional analysis reveals that the preferred source direction for this factor is southeast (SE) for Xiaogang and northwest (NW) for Linyuan, reflecting the locations of refinery facilities relative to each monitoring site (Fig. 4).

c) Industrial fugitive emissions

Isopentane and n-pentane are recognized tracers of natural gas operations (Gilman et al., 2013) or gasoline vapor emissions (Gentner et al., 2009). In our PMF results, both species showed elevated concentrations, indicating a strong contribution from fugitive sources (Fig. 3). Because isopentane and n-pentane exhibit similarly OH reaction rates (Atkinson, 1986), their ratio (iC_5/nC_5) is commonly used to identify emission sources (Bourtsoukidis et al., 2019). Accordingly, we examined this ratio across all sites using the PMF-resolved concentration of species from factor profile output to reveal their distinct relationship between isopentane and n-pentane.

Many studies report that an iC_5/nC_5 ratio in the range of approximately 0.8–1.1 is characteristic of oil & natural gas operations or raw-gas emissions (Gilman et al., 2013; Thompson et al., 2014; Swarthout et al., 2013; Gilman et al., 2010). In our analysis, the iC_5/nC_5 ratio was consistently <1 across the sites

and seasons, with site-specific seasonally mean values of 0.53 ± 0.02 at Linyuan, 0.76 ± 0.06 at Xiaogang, and 0.87 ± 0.10 at Chaozhou, all within or below the typical oil & natural gas range. The Kaoping region hosts only downstream industrial activities—such as refining, petrochemical processing, and feedstock production—rather than upstream extraction. Therefore, this factor was attributed to industrial fugitive emissions, likely originating from petrochemical processing units, storage tanks, and refinery-related leakage. The lowest ratio at Linyuan reflects a very local, fresh fugitive leak from proximate refinery/petrochemical sources. In contrast, the downwind receptor (Chaozhou) or the mixed urban-industrial area (Xiaogang) can result in higher ratios.

The PMF-resolved time series of industrial fugitive emission at all three sites—Xiaogang, Linyuan, and Chaozhou—exhibit a stable, low-level temporal pattern characteristic of continuous industrial fugitive emission sources across all seasons (Fig. S5). Occasional minor peaks occurred, with slightly higher values at Xiaogang and Linyuan than at Chaozhou at times, but no major episodic events were observed. This pattern underscores the nature of fugitive pollution, which remains a minor and relatively steady contributor to ambient NMHC levels year-round.

CPF analysis further reveals distinct spatial and seasonal patterns. At Linyuan and Xiaogang, elevated CPF values are associated with winds from the N-NW, and SE-SSE sectors, respectively, suggesting that elevated concentrations are most likely to occur under these prevailing wind conditions (Fig. 4). Winter and spring generally show slightly higher CPF values compared with summer and fall, particularly at these industrial sites, reflecting seasonal variations in atmospheric transport or emission dynamics.

In contrast, Chaozhou consistently displays low CPF values and the lowest NMHCs abundance across all seasons and wind directions, reflecting its rural setting, lack of industrial activity, and its downwind position relative to Xiaogang and Linyuan. The combination of weaker PMF-resolved timeseries (Fig. S5) and nearly uniform ratios of pentane isomers (0.87 ± 0.10) indicates that fugitive emissions reaching Chaozhou are largely diluted and regionally transported rather than locally generated. The winter enhancement is also consistent with the compositionally altered profile observed at Chaozhou (Fig. S4a), where atmospheric processing during transport and seasonal stagnation modifies the alkane distribution while retaining the broader characteristics of industrial fugitive emissions. Overall, the temporal and directional indicators confirm that Chaozhou is primarily influenced by diluted, downwind industrial fugitive emissions, with local contributions becoming detectable only under wintertime stagnation.

d) Mixed factor

In this study, distinguishing between vehicular and solvent-related emissions proved challenging, primarily because Kaohsiung City hosts large-scale petrochemical complexes, shipyards, and harbor facilities. Our PMF analysis was unable to resolve these sources as distinct factors but instead appropriately captured this complexity under a single, mixed source factor (Fig. 3). This likely reflects the complex emission environment of the region and possibly the proximity in distance of these source types, where vehicular activities and solvent usage co-occur, contributing overlapping NMHC species

such as toluene, benzene, ethylbenzene, etc (Chang et al., 2003). A major limitation in separating these sources is the absence of key tracers, such as 2,2,4-trimethylpentane (Huang and Hsieh, 2019), 2,3-dimethylbutane as recognized tracer of motor vehicle exhaust (Chang et al., 2004), or such as methyl tert-butyl ether (MTBE), as an indicator for vehicle exhaust or evaporation (Rubin et al., 2006; Chang et al., 2003; Lin et al., 2005), which makes it challenging to fully separate and resolve vehicle emissions. Another limitation is that CO, a commonly used tracer of combustion sources (Huang and Hsieh, 2019), was considered in the test PMF runs; however, its diagnostic value was restricted in the Kaoping region because multiple overlapping CO sources (e.g., traffic, industrial, residential burning, etc.) all contributed to elevated CO levels. As a result, the PMF model grouped vehicles and solvent-related emissions into a single mixed factor, reflecting the complex emission environment and overlapping NMHC signatures.

As a result, the mixed source factor exhibits contributions from both vehicular emissions and solvent-related industrial activities. Cai et al. (2010) reported that ethylene and propylene are major products of internal combustion engines, and both were present in our mixed factor. Additionally, acetylene—a known tracer of incomplete combustion—along with toluene, benzene, and m,p-xylene, typify vehicular emissions, further supporting the presence of traffic-related contributions (Nelson and Quigley, 1984; Baker et al., 2008; Liu et al., 2008a; Xu et al., 2017). Cyclopentane, 2-methylpentane, and methylcyclopentane are primarily markers of evaporation or unburned fuel from vehicles, rather than direct combustion products. Isoprene may also be present in vehicle exhaust, especially under conditions of incomplete combustion (e.g., cold starts, older engines, or engines lacking effective emission controls) (Nakashima et al., 2010; Park et al., 2011; Zou et al., 2019) or from tire wear (Jung and Choi, 2023). Moreover, the elevated contribution of heavier aromatic compounds (Fig. 3) suggests a further influence from diesel truck exhaust (Wang et al., 2024). The frequent presence of heavy-duty diesel trucks transporting steel, chemicals, machinery, and other goods was a common sight on the roads of Xiaogang and Linyuan, serving as the logistical backbone for multiple heavy industries in the region. Importantly, toluene is the dominant compound in the mixed factor, especially in Xiaogang, which provides a key constraint on source interpretation. The elevated toluene contribution points primarily to substantial solvent usage, as toluene is widely employed in paints, adhesives, coatings, and various cleaning agents, and chemical manufacturing processes common in industrial zones, along with ethylbenzene, m,p-xylene, n-hexane, and 1,2,4-trimethylbenzene (Wu et al., 2016; Shen et al., 2018; Shao et al., 2016). Together, the combined presence of combustion tracers, evaporative fuel markers, and solvent-related aromatics demonstrates that this factor represents a true mixture of vehicular exhaust and industrial solvent usage, with toluene-dominated solvent emissions (Bari and Kindzierski, 2018), serving as a major driver of its chemical profile. This mixed source factor highlights gaps in current emission inventories and underscores the need for improved, locally speciation-resolved data to support future research in this region.

By observing PMF-resolved time series (Fig. S5), the mixed factor exhibits strong seasonality, with its contributions peaking in winter, reaching the lowest levels in spring and summer, and rising

again in the fall. Xiaogang and Linyuan consistently display higher values than Chaozhou, especially during peak winter and late fall, highlighting the greater influence of industrial and traffic activities near these sites. While generally lower and more consistent, Chaozhou still shows some variability, indicating a minor but persistent influence from mixed sources. Interestingly, the mixed source factor often demonstrates a weekly concentration pattern characterized by elevated weekday levels and lower concentrations on weekends (Baidar et al., 2015; Pollack et al., 2012), further supporting the contribution from traffic-related emissions.

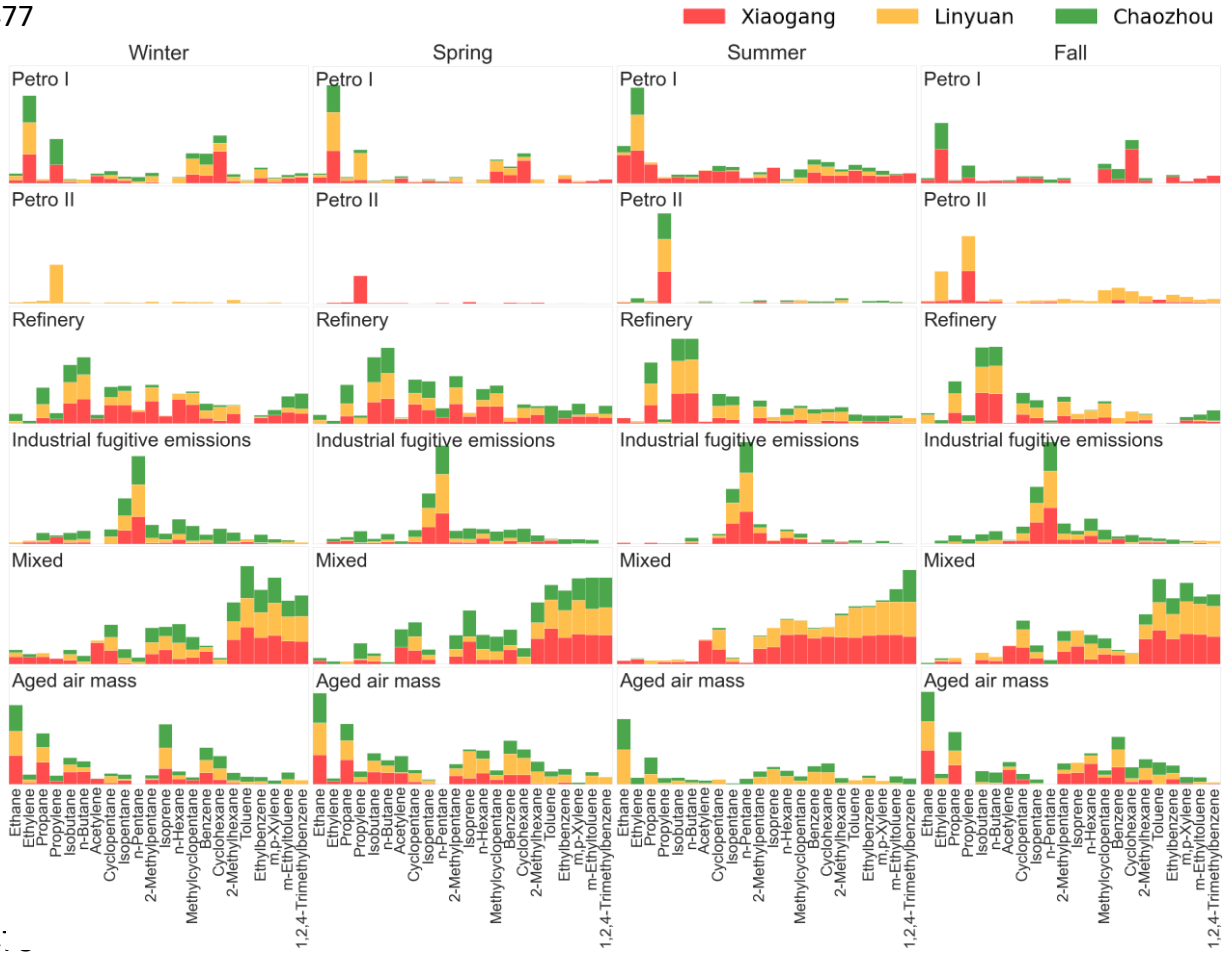

Figure 3: Summary of common source profiles of NMHC at the three sites in 2024. This figure presents the percentage contribution of six common source factors (Petro I, Petro II, Refinery, Industrial fugitive emissions, Mixed, and Aged air mass) to the total NMHC burden at three monitoring sites: Xiaogang (red), Linyuan (orange), and Chaozhou (green) across four seasons (Winter, Spring, Summer, and Fall). Each panel represents a specific source factor and season combination. The stacked bars within each panel show the relative contribution of NMHC species to that source factor. Consistent source profiles of fingerprint species were observed across seasons and at all three monitoring sites, underscoring the robustness of the PMF results.

Across all seasons, CPF values for the mixed factor remain relatively stable and uniform, suggesting that the contributing sources are predominantly local and affected by winds from multiple directions. However, during the fall, there is a noticeable increase in CPF values from the NW and NNW

sectors, corresponding with the onset and intensification of the northeastern monsoon (Fig. 4). This shift results in more frequent and stronger winds from these directions, enabling enhanced transport from upwind or regional sources and producing more pronounced CPF values from NW and NNW. Meanwhile, the elevated time series contributions observed during winter are likely due to accumulation in the atmosphere, driven by a lower mixing layer height, which promotes the buildup of locally emitted pollutants (Fig. S5).

e) Aged air mass factor

The aged air mass factor was characterized by a dominant presence of low-reactivity, long-lived (NMHCs), including ethane, propane, acetylene, and benzene (Fig. 3). These compounds are sufficiently stable to survive long-range atmospheric transport due to their relatively slow reaction rates with hydroxyl (OH) radicals. The atmospheric chemical lifetimes of these VOCs range from several days to months, allowing them to persist in the environment and become enriched over time (Atkinson and Arey, 2003; Lau et al., 2010). Such compositional features suggest that the aged air mass is primarily influenced by secondary and transported sources rather than recent local emissions. Ethane, in particular, often dominates this factor due to its long atmospheric lifetime, and its strong presence aligns with findings from previous studies (Chen et al., 2010; Li et al., 2015). Similarly, benzene and acetylene are frequently observed in aged air masses, consistent with the findings of Wu et al. (2016), suggesting regional transport rather than local fugitive emissions as their primary source.

The PMF-resolved time series of the aged air mass factor reveals distinct seasonal trends. Contributions from aged air mass rise in late fall, peaking during winter, most notably at Xiaogang and Linyuan (Fig. S5, the red and orange lines). This elevated influence persists into spring before gradually declining, a pattern that closely mirrors the strengthening and subsequent weakening of the northern monsoon. While Chaozhou is located further inland, its aged air mass time series remains comparable to those at Xiaogang and Linyuan, though slightly lower in magnitude. This suggests that Chaozhou is still significantly influenced by long-range transport and potentially nearby sources from the vicinity areas. These spatial differences underscore the critical role of seasonal wind direction and site location in shaping the transport and accumulation of aged air masses across the sites.

Analysis of CPF values further supports these findings, with generally higher values observed from the NW to N wind sectors (Fig. 4), consistent with the prevailing northern monsoon during late fall through spring. Xiaogang and Linyuan display pronounced CPF peaks in these directions, reinforcing their susceptibility to long-range transport and downwind positioning during the monsoon. This pattern aligns well with the elevated time series signals observed at these sites during winter and early spring.

By contrast, Chaozhou exhibits lower CPF values and less direct influence from the northern monsoon. Instead, the CPF values at Chaozhou are enhanced under western wind conditions, suggesting that local factors, such as inland positioning and the influence of sea–land breeze circulation, modulate its exposure to aged air mass transported from Xiaogang and Linyuan. Fig. S6 further supports this observation as it shows the wind profile during day & night in alignment with the sea-land breeze pattern

at Kaohsiung. Taken together, these patterns highlight the interplay of regional transport, seasonal meteorology, and site-specific geography in determining the concentration and source influence of aged air masses across the study area. In summary, the six common factors—Petro I, Petro II, refinery, industrial fugitive emissions, mixed, and aged air mass—represent the dominant anthropogenic and transported NMHC sources across the Kaoping region.

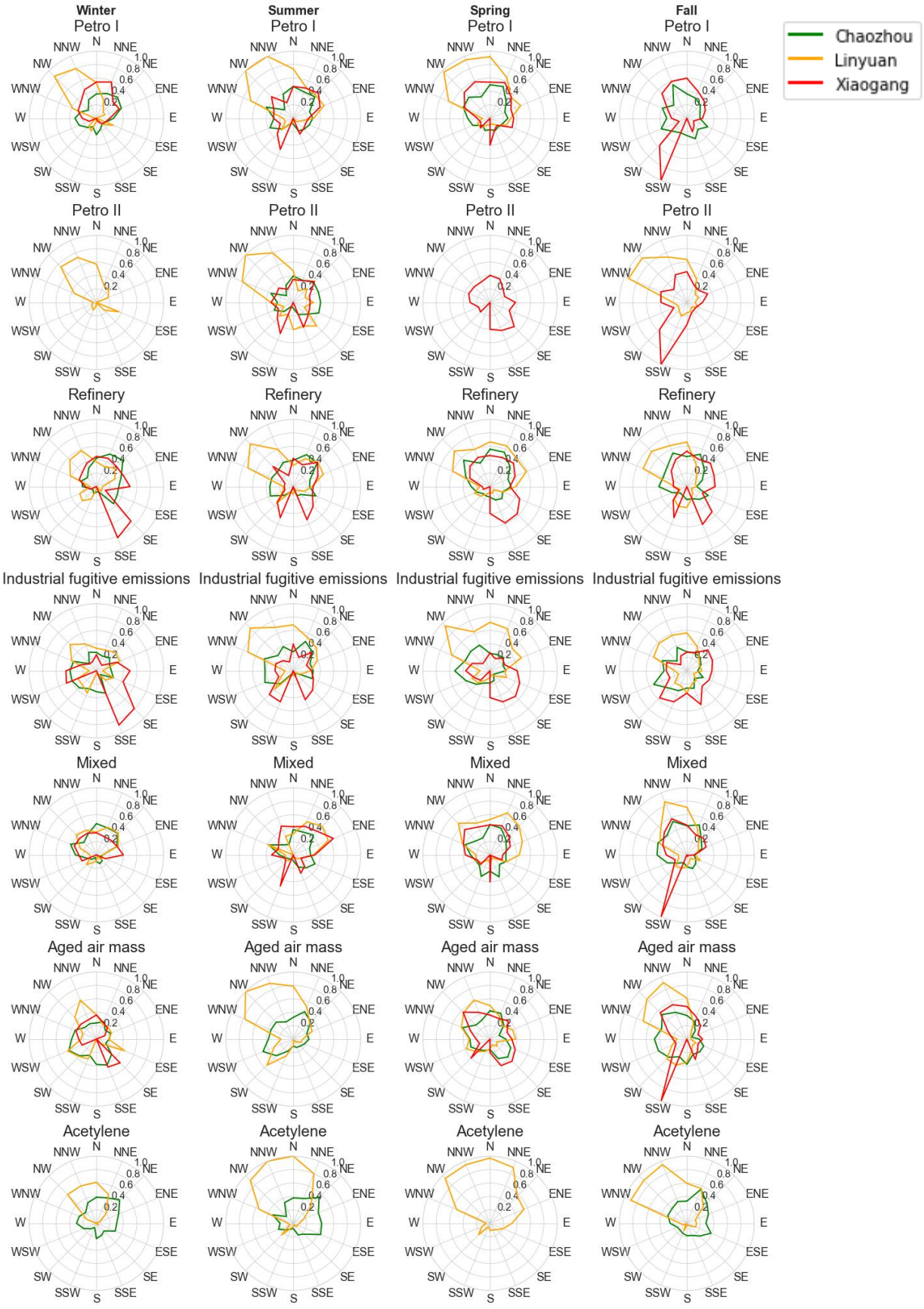

533 **Figure 4: CPF results viewing the direction for the highest 30% of factor contribution**

3.3.2 Distinct sources

a) Biogenic factor

The PMF results at Chaozhou identify a biogenic factor dominated by isoprene, with contributions present in both summer and fall (Fig.5). Temporal patterns (Fig. S7a,b) show that isoprene levels are substantially higher and more variable in summer, consistent with strong temperature and solar radiation dependence of biogenic isoprene emissions (Zeng et al., 2023; Vettikkat et al., 2023). These conditions are more intense and sustained during the summer months in southern Taiwan, and the surrounding agricultural landscape provides a plausible source. The pronounced late-morning to mid-afternoon peak (10:00–15:00) further supports a photosynthetically driven biogenic origin.

Notably, the biogenic factor profile also contains co-emitted VOCs, forming a mixed-species profile in which the isoprene signature is less distinct in summer but appears cleaner and more purely biogenic in fall. The observation is consistent with emerging evidence that urban isoprene budgets can include other non-biogenic sources (Peron et al., 2024), or traffic emissions (Chang et al., 2014; Hsieh et al., 2017). Residential biomass burning is another plausible contributor that can modify ambient mixtures during episodic events (Desservettaz et al., 2023). Given the agricultural setting at Chaozhou, biomass burning is likely a significant local source.

The CPF analysis (Fig. S7c) further supports a local and regionally distributed source profile, with increased conditional probabilities from the SSW and NW sectors during both seasons. These wind directions correspond with vegetated and agricultural areas surrounding the site, reinforcing the role of nearby land cover in influencing isoprene levels. However, the non-directional component and broader sector coverage also support additional inputs from anthropogenic sources, particularly traffic emissions and biomass burning. The seasonal and diurnal behaviors highlight the sensitivity of isoprene to environmental drivers and the complex nature of its mixed-source regions, such as Chaozhou.

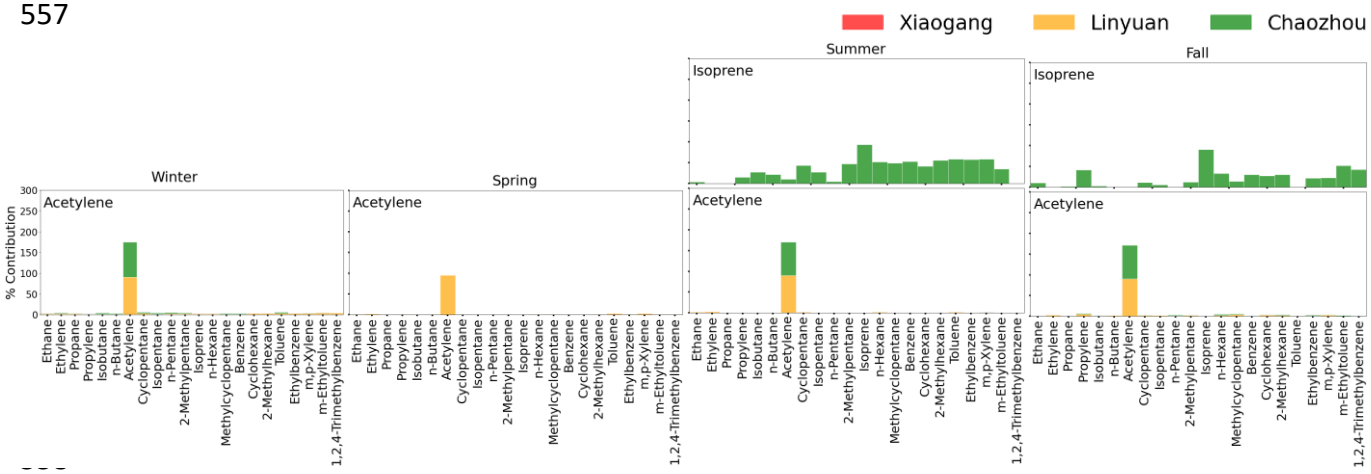

Figure 5: Distinct source profiles of NMHC at the three sites in 2024

b) Acetylene factor

Acetylene (C_2H_2) is a highly flammable hydrocarbon gas and is mainly used as a fuel gas for oxy-acetylene welding, cutting, brazing, and soldering. On the other hand, the filling process for high-pressure cylinders is also prone to leaking. From the PMF results in Fig. 5, there is a resolved factor for

564 the single species of acetylene and no other accompanying species source at Linyuan and Chaozhou,
565 suggesting that acetylene is a pronounced local source, which is consistent with the prior knowledge of
566 the acetylene filling plant in the region.
567 PMF-resolved time series of the acetylene factor reveals a temporal pattern, with elevated
568 contributions during winter and fall, and generally lower levels in summer (Fig. S5). These variations
569 are likely driven by meteorological influences, such as enhanced atmospheric stability and reduced
570 boundary layer height in colder months, which favor the accumulation of locally emitted pollutants. In
571 contrast, stronger vertical mixing and photochemical degradation in summer likely contribute to the
572 overall reduction in acetylene levels during this period.
573 Complementary insights are provided by the CPF analysis, which highlights the directional
574 characteristics of acetylene sources. Seasonal CPF polar plots show that Linyuan (orange) consistently
575 exhibits strong directional signals, with the highest probabilities originating from the NW–NE across
576 all seasons. This directional consistency supports the presence of a persistent local source to the north
577 of the site–aligned with the known location of an acetylene filling plant in the region. The elevated CPF
578 values in these wind sectors reinforce the interpretation that the PMF-resolved acetylene factor reflects
579 a geographically localized emission source, with its observed variability driven more by meteorological
580 transport conditions than by changes in source activity. In contrast, no acetylene factor was resolved at
581 Xiaogang, and this absence is consistent with its prevailing wind patterns. Seasonal wind rose data show
582 that Xiaogang is predominantly influenced by W and NW winds (Fig. S8)—directions that do not align
583 with the position of the acetylene source near Linyuan, which lies to the southeast of Xiaogang. As a
584 result, the site remains largely unaffected by emissions from the filling facility.
585 Chaozhou is an agricultural area that leads to open-field biomass burning beginning in late summer
586 and extending to the rest of the year. Acetylene is an emission from incomplete combustion processes,
587 such as biomass burning (Burling et al., 2010; Wang et al., 2014), and therefore exhibits its strongest
588 summer spikes and weaker, intermittent fall and winter contributions (Fig. 2a, Fig. S1). This seasonal
589 pattern reflects intermittent but intensified combustion activities rather than continuous emissions.
590 Consequently, although PMF resolves an acetylene-rich factor at both Linyuan and Chaozhou, its
591 contribution at Chaozhou is much lower (Fig. S5). Unlike Linyuan—where a known nearby acetylene
592 filling plant provides a persistent local source—Chaozhou is influenced mainly by diffuse biomass
593 burning and other small-scale, variable combustion activities. The absence of a strong directional signal
594 in the CPF analysis for Chaozhou further supports the interpretation that acetylene in Chaozhou
595 originates from non-point or variable sources rather than a single dominant emitter.
596 **3.4 PMF-Trigger back trajectory integration**
597 It is noteworthy that an acetylene-related factor was clearly resolved in the PMF results, especially
598 for Linyuan but not for Xiaogang. This outcome aligns well with the raw PAMS observations, where
599 acetylene concentrations at Linyuan are markedly elevated, often exhibiting sharp spikes reaching
600 several hundred ppb (Fig. S1), especially in winter. In contrast, levels at Xiaogang remain consistently
601 low, rarely exceeding 20 ppb. The resolution of the acetylene factor at Linyuan can be attributed to the

high signal-to-noise ratio in the PAMS data, where sharp and frequent concentration spikes provided a clear signal for PMF to distinguish this source from others, resulting in a well-defined temporal profile that closely matched the observed data. This supports the reliability of PMF in capturing source-specific signatures when driven by strong observational input.

Beyond factor profiles and species contributions, the PMF-resolved acetylene factor at Linyuan also resulted in a well-defined temporal profile that closely matched the observed data. Figure 6a demonstrates this consent with a coefficient of determination (R^2) exceeding 0.99. This high level of agreement underscores the ability of PMF to cleanly resolve the profile dominated by a single species, acetylene, and to accurately reproduce the temporal variability of pollutant levels. While many PMF studies focus primarily on profile interpretation, this study demonstrates that time series validation can provide an additional, rigorous layer of confidence in the factor identification—highlighting the robustness of the PAMS dataset and the reliability of the PMF analysis. As a result, acetylene serves as an intrinsic reference species, providing an internal check on the PMF analysis.

Because the acetylene events at Linyuan are extremely distinct, a triggered back-trajectory analysis was conducted to investigate their source locations. This analysis used observational data from the monitoring station as input, under the assumption that the local wind field was representative of the broader surrounding area. The model was configured to calculate air parcel trajectories 15 minutes backward from the observation site. Geographic Information System (GIS) tools and Google Maps API were used to spatially visualize the trajectories and identify potential emission hotspots through trajectory receptor pattern overlay analysis. Setting an appropriate concentration threshold is critical for isolating representative pollution events. If the threshold is too low, resulting trajectories may be overly dispersed, making source identification difficult. Conversely, a threshold set too high may highlight only extreme events, which may not represent typical source behavior. This analysis applied a threshold of 96.85 ppb (95th quantile) to ensure that only significant acetylene events were considered.

The overlay of multiple high-concentration trajectories consistently pointed to an area near the acetylene filling facility (Fig. 6). Although the backward trajectories do not align perfectly with the suspected emission source, this deviation is likely due to the influence of complex coastal meteorology that can affect low-level air parcel paths, especially under transitional wind conditions. Moreover, the trajectory model may not fully capture local turbulence and terrain effects, contributing to the observed offset. Despite this, the temporal patterns of peaked acetylene, combined with the site's position relative to the dominant wind direction, support the likely influence of the identified source. These findings demonstrate the value of high-resolution PAMS data in capturing pollutant events and reinforce the consistency between observational measurements and PMF-based source apportionment. Finally, the back-trajectory method, particularly when applied in a triggered mode during elevated events, offers enhanced spatial resolution and source identification capabilities that complement and extend beyond PMF results. Further trajectories are also run for Chaozhou, which supports the hypothesis that the high peak in August originates from local sources, indicating an intermittent episode peak from biomass burning in such a highly agricultural landscape (Fig. S1). This interpretation is further strengthened by

the trajectory analysis (Fig. S9), which shows locally originating and spatially scattered air mass pathways around the monitoring site.

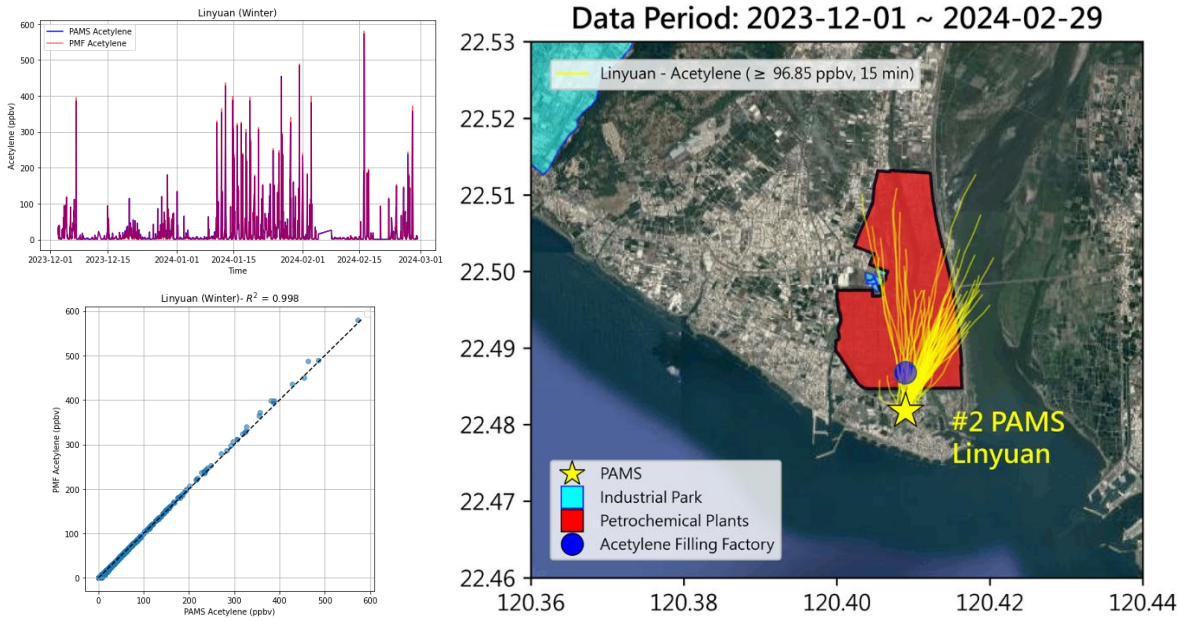

a) Agreement of PAMS and PMF-resolved factor

b) Triggered back trajectory

Figure 6: The acetylene factor at Linyuan, (a) time series comparison and (b) Triggered back trajectory analysis of spike levels. Base map from Google Maps (Map data ©2025 Google).

3.5 Quantitative estimates of source contributions.

The differences in source contribution across the three sites are not arbitrary but rather reflect the distinct roles each monitoring station plays within the regional emission landscape. Linyuan functions as a source site because it is home to major refinery and petrochemical facilities. Xiaogang, by contrast, presents a mixed urban-industrial environment, while Chaozhou acts as a downwind receptor site in a predominantly rural setting. Since many NMHC species originate from multiple source types, the resolved factors were grouped into broader categories: petroleum industry (including petro I & II, refinery, and industrial fugitive emissions), mixed, aged air mass, acetylene, and biogenic.

Figure 7 illustrates the seasonal contribution of these grouped sources. Interestingly, the petroleum-related source contribution is most prominent (33-71%), especially at Xiaogang, despite Linyuan being the location of core petrochemical activities. This apparent contradiction can be explained by local meteorological conditions—particularly prevailing winds and sea–land breeze effects—which frequently transport emissions from the surrounding industrial corridor toward Xiaogang. These wind-driven dynamics create a receptor–source relationship, wherein Xiaogang accumulates both locally emitted and regionally transported pollutants. In contrast, Linyuan shows a strong signal from the acetylene factor, pointing to localized activities with distinct point-source characteristics. Meanwhile, Chaozhou's elevated aged air mass contribution underscores its role as a downwind receptor site.

Aged air masses consistently influence all sites and seasons, with contributions ranging from 12% to 30%. Chaozhou, in particular, exhibits higher contributions—up to 30% in spring and above 27% in winter and fall, while summer shows the lowest levels. Its inland, rural settings with limited local

industrial activity suggest that the site primarily receives aged air masses transported from upwind regions. Supporting this interpretation, evidence from CPF analysis (Fig. 4 and Fig. S6) highlight the role of local recirculation driven by sea-land breeze, which enhances the aging of air masses near the site. Additionally, long-range transport under prevailing winter monsoon winds further reinforces the elevated aged air signal observed at Chaozhou. At the same time, Xiaogang emerged as the second contributor of aged air mass, with notable peaks in winter, spring, and fall. As a result, the three sites with their unique source-receptor characteristics produce very dynamic source apportionment results that vary in season and locations.

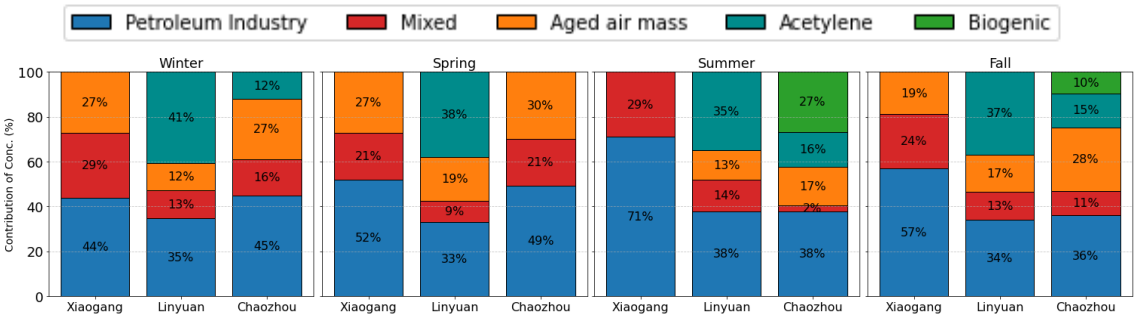

Figure 7: Seasonal contributions of grouped source factors at each site. Details of the eight resolved factors are provided in Fig. S10

3.6 OFP dynamics under varying ozone conditions

Given that photochemical reactions predominantly occur during daylight hours, the OFP was calculated exclusively for daytime periods, defined using sunrise and sunset times, derived from astronomical data tailored to each station's geographic locations and observation dates. Seasonally averaged OFP values attributed to source factors were highest at Xiaogang (113.20 ± 23.60 μg/m³), followed by Linyuan (102.73 ± 40.93 μg/m³), and lowest at Chaozhou (65.38 ± 9.00 μg/m³), as shown in Fig. S11. Spatially, the distribution of OFP contributions varied consistently with their previously identified roles. Notably, while petroleum-related sources exhibited the highest contributions in terms of concentration, they were not always the leading contributors to OFP. For example, at Xiaogang, the petroleum factor ranked second in OFP, overtaken by the mixed source factor (Fig. S11). This is primarily due to the presence of highly reactive species—such as aromatics—in the mixed source profile, which significantly elevates its OFP despite relatively lower concentrations. In Xiaogang, the mixed source was the dominant contributor to OFP during most seasons, with petroleum-related sources only surpassing it in summer. To further explore source contributions under varying ozone pollution conditions, the dataset was classified based on the maximum daily 8-hour average (MDA8) ozone concentrations: days with MDA8 larger than 60 ppb were designated as pollution (POL) days, and those with MDA8 between 40 and 60 ppb as moderate pollution (MOD) days. OFP was recalculated accordingly, and the percentage contributions of each source factor are presented in Figure 8. The comparison between POL and MOD days reveals notable shifts in source influence across the region.

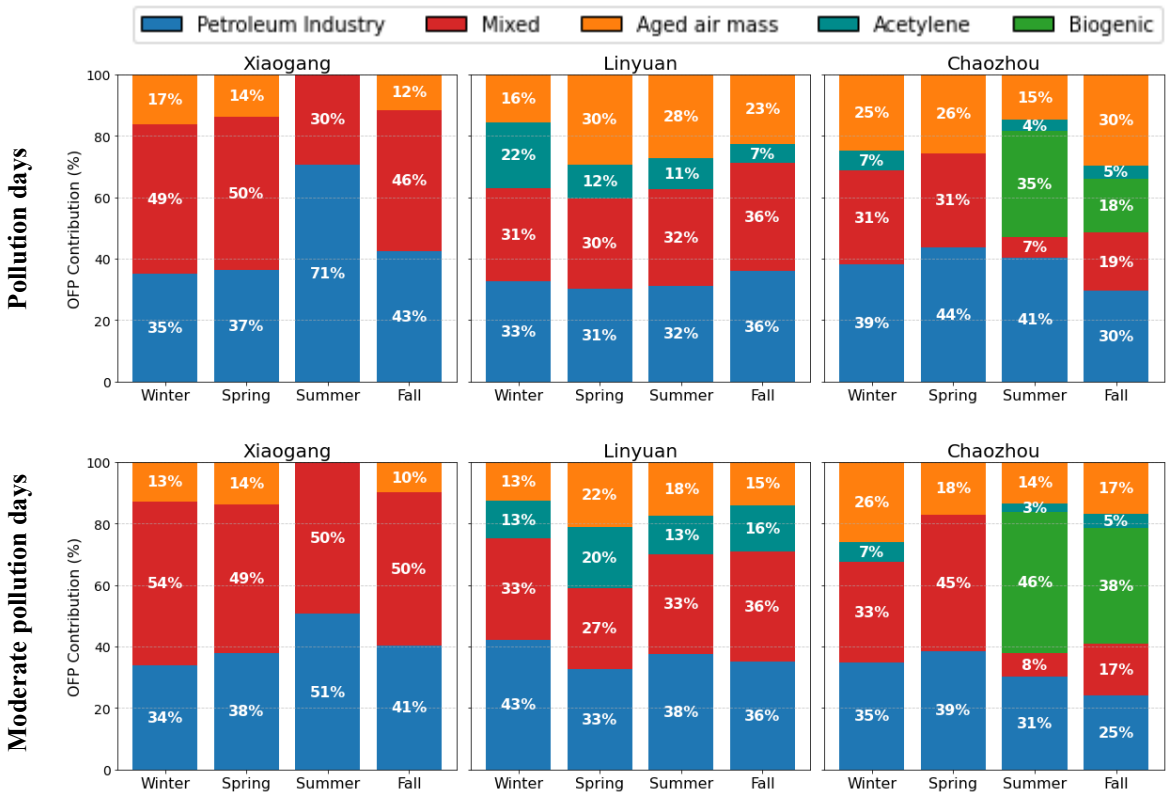

Figure 8: Corresponding daytime OFP during pollution and moderate pollution days of ozone

Mixed and petroleum-related sources consistently contribute a substantial portion of OFP under both conditions. For example, mixed sources are the dominant contributor, particularly at urban-industrial sites such as Xiaogang, underscoring their strong role in ozone precursor formation even during less intense ozone conditions. Meanwhile, petroleum-related sources showed an enhanced contribution at Linyuan, suggesting a stronger association with moderate ozone levels. Overall, large-scale industrial and traffic-related emissions (petro-, mixed, and acetylene-related) provide a highly reactive precursor condition conducive to ozone formation across Xiaogang and Linyuan areas, consistent with their dense industrial landscape.

Under moderate-ozone conditions, the mixed-source factor contributes the largest share of OFP. These episodes are frequently associated with lower wind speeds and reduced mixing heights (Aacog, 2015), favoring the accumulation of locally emitted species from traffic, solvents, and smaller-scale industrial activities. The coexistence of these emissions provides a balanced supply of reactive aromatics and olefins, sustaining ozone production even in the absence of strong photochemical aging. This pattern reflects the VOC-limited photochemical environment prevalent in southern Taiwan, where ozone formation is more sensitive to reactive VOCs than to NOx levels (Chang et al., 2022), emphasizing that moderate-ozone episodes are primarily governed by local accumulation and NMHC composition. However, the mixed-source factor reflects overlapping characteristics of vehicular and solvent-related species. This incomplete separation introduces some uncertainty in source-specific attribution of OFP. Nevertheless, this overlap mirrors the reality of urban environments.

Meanwhile, the aged air mass factor exerted a notable influence on ozone pollution days, especially at downwind sites such as Linyuan and Chaozhou. This highlights the role of regional

transport and atmospheric aging in shaping local ozone levels. The elevated OFP from aged air mass during pollution events suggests that some reactive NMHCs are transported from upwind areas after undergoing photochemical processing rather than emitted locally. Importantly, aged air masses may also carry ozone itself, effectively elevating the background ozone concentration and providing a higher baseline upon which local photochemical production builds (Nguyen et al., 2025). This dual role—delivering both precursors and ozone—can intensify pollution episodes.

At Chaozhou, biogenic emissions made a significant contribution to the OFP, particularly during the summer and fall seasons. This reflects the release of isoprene from surrounding agriculture and vegetation landscape, which can react rapidly with transported NOx to form ozone. The biogenic influence was especially evident during moderate ozone days, suggesting that these episodes are more sensitive to the combined effects of natural emissions, transported NOx, and local atmospheric chemistry. This underscores the importance of considering seasonal and spatial dynamics in emission control strategies—especially in areas like Xiaogang and Linyuan, where anthropogenic and biogenic sources interact synergistically to elevate ozone levels.

Regarding chemical speciation, the dominant OFP contributors across all sites and seasons were aromatics, alkanes, and alkenes, owing to their high photochemical reactivity. Aromatics—particularly toluene and m,p-xylene (Fig. S12)—accounted for 32–61% of the OFP during moderate pollution days, with the highest contributions observed at Xiaogang. Alkanes, primarily ethane, contributed 20–35%, with similar levels at Xiaogang and Linyuan, and slightly higher at Chaozhou during polluted periods. Alkenes, especially propylene, contributed 15–24%, peaking at Xiaogang during pollution days and at Linyuan during moderate ozone conditions. Additional contributions were observed from ethyne—notably at Linyuan—and from isoprene at Chaozhou, where they played a more prominent role under moderate ozone conditions. Although acetylene has a relatively low MIR value, its large emission volume—primarily from the filling plant—still led to significant OPF contribution downwind.

The persistence of higher OFP contributions during moderate ozone days indicates that precursor control should not be limited to pollution events alone. Effective ozone management, therefore, requires a multi-faceted approach that integrates anthropogenic and biogenic sources, seasonal variability, and transportation influences to design more adaptive, location-specific mitigation policies.

4. Conclusion

This study provides a comprehensive analysis of NMHC concentrations and their sources across three distinct sites in southern Taiwan: Linyuan, Xiaogang, and Chaozhou. The findings revealed significant spatial heterogeneity in NMHC concentrations and source profiles, reflecting the diverse land use and industrial activities across the region. Linyuan, a dense industrial landscape, exhibited the highest average NMHC concentrations, followed by the mixed urban-industrial environment of Xiaogang, with the lowest levels observed at the predominantly agricultural site of Chaozhou. PMF analysis identified eight distinct source factors contributing to NMHCs at the three sites: petrochemical I & II, refinery, industrial fugitive emissions, mixed (vehicular/solvent), aged air mass, acetylene, and biogenic.

The strength of this study lies in the use of PMF-resolved time series output, allowing for the identification of concentration spikes indicative of episodic emission events. The acetylene factor, in particular, showed excellent agreement with PAMS observations (R^2 over 0.99), which triggered targeted back-trajectory analyses. These consistently traced emissions to a nearby acetylene filling facility north of the Linyuan industrial area. The integration of PMF-resolved time series data with trajectory modeling reinforces the credibility of the source apportionment results and underscores the high quality and temporal resolution of the observational data. It enabled a more precise attribution of pollution sources and facilitated the isolation and examination of individual pollution events.

In addition, this study explored the dynamics of OFP. They were calculated specifically for daytime periods—when photochemical activity is most pronounced. Seasonally averaged OFP was highest at Xiaogang (113.20 ± 23.60 μg/m³), followed by Linyuan (102.73 ± 40.93 μg/m³), and lowest at the downwind rural site Chaozhou (65.38 ± 9.00 μg/m³). Although petroleum-related sources contributed the largest fraction of NMHC concentrations, the mixed source factor—enriched in highly reactive species such as aromatics and olefins—often dominates the OFP, particularly at Xiaogang. Under moderate-ozone conditions (MDA8 40–60 ppb), the factor became the principal driver of ozone formation, consistent with local accumulation under stagnant meteorological conditions and limited vertical mixing. The coexistence of both reactive aromatics and olefins within this factor sustained ozone production despite weak photochemical aging, reflecting a VOC-limited regime typical of southern Taiwan. Across ozone pollution levels, petroleum and mixed sources remained dominant, but their relative influence varied with site characteristics. Mixed sources exerted stronger effects during moderate-ozone episodes at urban–industrial locations, whereas petroleum-related sources dominated in Linyuan under similar conditions. These results suggest that frequent, moderate-ozone episodes are primarily driven by locally accumulated reactive NMHCs. This pattern may also reflect the early impacts of emission control measures, which are more effective under high-pollution conditions but less so during moderate episodes. Given their higher occurrence, moderate pollution episodes still offer valuable insights into the interplay between local accumulation, VOC reactivity, and emission composition that governs ozone formation in the region.

Overall, this study demonstrates the strength of a refined source apportionment approach using multi-site, year-round, high-frequency NMHC measurements, each reflecting distinct source–receptor dynamics. The findings offer a more comprehensive spatiotemporal understanding of ozone formation mechanisms and provide a scientific basis for coordinated control of mobile, solvent-related, and petroleum-associated emissions across southern Taiwan.

Data availability: All raw data can be provided by the corresponding authors upon request.

Author contributions: JLW and CHW formed the conceptualization; HCH developed the model code and performed the modeling; DHN and HCH analyzed the data; DHN wrote the original draft; JLW, NHL, CHW, MCL, and DHN reviewed and edited the manuscript.

Competing interests: The authors declare that they have no conflict of interest.

References

AACOG: Conceptual Model, Ozone Analysis of the San Antonio Region, Updates through Year 2014,

https://aacog.gov/sites/default/files/2022-07/Conceptual%20Model%2C%20Ozone%20Analysis%20of%20the%20San%20Antonio%20Region%2C%20Updates%20through%20Year%202014.pdf?utm_source=chatgpt.com, 2015.

Atkinson, R.: Kinetics and mechanisms of the gas-phase reactions of the hydroxyl radical with organic compounds under atmospheric conditions, Chemical Reviews, 86, 69-201, 1986.

Atkinson, R. and Arey, J.: Atmospheric degradation of volatile organic compounds, Chemical reviews, 103, 4605-4638, https://pubs.acs.org/doi/full/10.1021/cr0206420, 2003.

Baidar, S., Hardesty, R., Kim, S. W., Langford, A., Oetjen, H., Senff, C., Trainer, M., and Volkamer, R.: Weakening of the weekend ozone effect over California's South Coast Air Basin, Geophysical Research Letters, 42, 9457-9464, https://doi.org/10.1002/2015GL066419, 2015.

Baker, A. K., Beyersdorf, A. J., Doezema, L. A., Katzenstein, A., Meinardi, S., Simpson, I. J., Blake, D. R., and Rowland, F. S.: Measurements of nonmethane hydrocarbons in 28 United States cities, Atmospheric Environment, 42, 170-182, https://doi.org/10.1016/j.atmosenv.2007.09.007, 2008.

Bari, M. A. and Kindzierski, W. B.: Ambient volatile organic compounds (VOCs) in Calgary, Alberta: sources and screening health risk assessment, Science of the Total Environment, 631, 627-640, https://doi.org/10.1016/j.scitotenv.2018.03.023, 2018.

Bourtsoukidis, E., Ernle, L., Crowley, J. N., Lelieveld, J., Paris, J.-D., Pozzer, A., Walter, D., and Williams, J.: Non-methane hydrocarbon (C 2–C 8) sources and sinks around the Arabian Peninsula, Atmospheric Chemistry Physics, 19, 7209-7232, 2019.

Burling, I., Yokelson, R. J., Griffith, D. W., Johnson, T. J., Veres, P., Roberts, J., Warneke, C., Urbanski, S., Reardon, J., and Weise, D.: Laboratory measurements of trace gas emissions from biomass burning of fuel types from the southeastern and southwestern United States, Atmospheric Chemistry Physics, 10, 11115-11130, 2010.

Buzcu, B. and Fraser, M. P.: Source identification and apportionment of volatile organic compounds in Houston, TX, Atmospheric Environment, 40, 2385-2400, https://doi.org/10.1016/j.atmosenv.2005.12.020, 2006.

Cai, C., Geng, F., Tie, X., Yu, Q., and An, J.: Characteristics and source apportionment of VOCs measured in Shanghai, China, Atmospheric Environment, 44, 5005-5014, https://doi.org/10.1016/j.atmosenv.2010.07.059, 2010.

Carter, W. P.: Development of the SAPRC-07 chemical mechanism, Atmospheric Environment, 44, 5324-5335, https://doi.org/10.1016/j.atmosenv.2010.01.026, 2010.

Chang, C.-C., Chen, T.-Y., Chou, C., and Liu, S.-C.: Assessment of traffic contribution to hydrocarbons using 2, 2-dimethylbutane as a vehicular indicator, Terrestrial Atmospheric Ocenanic Sciences, 15, 697-712, 2004.

Chang, C.-C., Lo, S.-J., Lo, J.-G., and Wang, J.-L.: Analysis of methyl tert-butyl ether in the atmosphere and implications as an exclusive indicator of automobile exhaust, Atmospheric Environment, 37, 4747-4755, https://doi.org/10.1016/j.atmosenv.2003.08.017, 2003.

Chang, C.-C., Wang, J.-L., Lung, S.-C. C., Chang, C.-Y., Lee, P.-J., Chew, C., Liao, W.-C., Chen, W.-N.,

and Ou-Yang, C.-F.: Seasonal characteristics of biogenic and anthropogenic isoprene in tropical–subtropical urban environments, Atmospheric environment, 99, 298-308, https://doi.org/10.1016/j.atmosenv.2014.09.019, 2014.

Chang, J. H.-W., Griffith, S. M., Kong, S. S.-K., Chuang, M.-T., and Lin, N.-H.: Development of a CMAQ-PMF-based composite index for prescribing an effective ozone abatement strategy: A case study of sensitivity of surface ozone to precursor VOC species in southern Taiwan, Atmospheric Chemistry Physics Discussions, 2022, 1-48, https://doi.org/10.5194/acp-23-6357-2023, 2022.

Chen, C.-H., Chuang, Y.-C., Hsieh, C.-C., and Lee, C.-S.: VOC characteristics and source apportionment at a PAMS site near an industrial complex in central Taiwan, Atmospheric Pollution Research, 10, 1060-1074, 2019.

Chen, C., Wang, L., Qin, Y., Zhang, Y., Zheng, S., Yang, Y., Jin, S., and Yang, X.: Voc characteristics and their source apportionment in the yangtze river delta region during the g20 summit, Atmosphere, 12, 928, https://doi.org/10.3390/atmos12070928, 2021a.

Chen, S.-P., Liu, W.-T., Hsieh, H.-C., and Wang, J.-L.: Taiwan ozone trend in response to reduced domestic precursors and perennial transboundary influence, Environmental Pollution, 289, 117883, https://doi.org/10.1016/j.envpol.2021.117883, 2021b.

Chen, S.-P., Liu, T.-H., Chen, T.-F., Yang, C.-F. O., Wang, J.-L., and Chang, J. S.: Diagnostic modeling of PAMS VOC observation, Environmental Science Technology, 44, 4635-4644, https://doi.org/10.1021/es903361r, 2010.

Chen, S.-P., Liao, W.-C., Chang, C.-C., Su, Y.-C., Tong, Y.-H., Chang, J. S., and Wang, J.-L.: Network monitoring of speciated vs. total non-methane hydrocarbon measurements, Atmospheric Environment, 90, 33-42, 2014.

Cheng, J.-O., Ko, F.-C., Lee, C.-L., and Fang, M.-D.: Atmospheric polycyclic aromatic hydrocarbons (PAHs) of southern Taiwan in relation to monsoons, Environmental Science Pollution Research, 23, 15675-15688, https://doi.org/10.1007/s11356-016-6751-9, 2016.

Chou, C. C. K., Lung, S.-C. C., Hsiao, T.-C., and Lee, C.-T.: Regional and Urban Air Quality in East Asia: Taiwan, in: Handbook of Air Quality and Climate Change, 1-38, https://doi.org/10.1007/978-981-15-2527-8_71-1, 2022.

Deng, Y.-M., Wu, H.-W., and Liao, H.-E.: Utilization intention of community pharmacy service under the dual threats of air pollution and COVID-19 epidemic: Moderating effects of knowledge and attitude toward COVID-19, International Journal of Environmental Research Public Health, 19, 3744, https://doi.org/10.3390/ijerph19063744, 2022.

Desservettaz, M., Pikridas, M., Stavroulas, I., Bougiatioti, A., Liakakou, E., Hatzianastassiou, N., Sciare, J., Mihalopoulos, N., and Bourtsoukidis, E.: Emission of volatile organic compounds from residential biomass burning and their rapid chemical transformations, Science of The Total Environment, 903, 166592, 2023.

Dong, Z., Zhang, D., Wang, T., Song, X., Hao, Y., Wang, S., and Wang, S.: Sources and environmental impacts of volatile organic components in a street canyon: Implication for vehicle emission, Science of

The Total Environment, 917, 170569, https://doi.org/10.1016/j.scitotenv.2024.170569, 2024.
Dumanoglu, Y., Kara, M., Altiok, H., Odabasi, M., Elbir, T., and Bayram, A.: Spatial and seasonal variation and source apportionment of volatile organic compounds (VOCs) in a heavily industrialized region, Atmospheric Environment, 98, 168-178, https://doi.org/10.1016/j.atmosenv.2014.08.048, 2014.
Finlayson-Pitts, B. and Pitts Jr, J.: Atmospheric chemistry of tropospheric ozone formation: scientific and regulatory implications, Air Waste, 43, 1091-1100, 1993.
Gentner, D. R., Harley, R. A., Miller, A. M., and Goldstein, A. H.: Diurnal and seasonal variability of gasoline-related volatile organic compound emissions in Riverside, California, Environmental Science Technology, 43, 4247-4252, 2009.
Gilman, J. B., Lerner, B. M., Kuster, W. C., and De Gouw, J.: Source signature of volatile organic compounds from oil and natural gas operations in northeastern Colorado, Environmental Science Technology, 47, 1297-1305, 2013.
Gilman, J. B., Burkhart, J. F., Lerner, B. M., Williams, E. J., Kuster, W., Goldan, P. D., Murphy, P. C., Warneke, C., Fowler, C., and Montzka, S. A.: Ozone variability and halogen oxidation within the Arctic and sub-Arctic springtime boundary layer, Atmospheric Chemistry Physics, 10, 10223-10236, 2010.
Gu, Y., Liu, B., Li, Y., Zhang, Y., Bi, X., Wu, J., Song, C., Dai, Q., Han, Y., and Ren, G.: Multi-scale volatile organic compound (VOC) source apportionment in Tianjin, China, using a receptor model coupled with 1-hr resolution data, Environmental Pollution, 265, 115023, https://doi.org/10.1016/j.envpol.2020.115023, 2020.
Guan, Y., Wang, L., Wang, S., Zhang, Y., Xiao, J., Wang, X., Duan, E., and Hou, L. a.: Temporal variations and source apportionment of volatile organic compounds at an urban site in Shijiazhuang, China, Journal of Environmental Sciences, 97, 25-34, https://doi.org/10.1016/j.jes.2020.04.022, 2020.
Guo, H., Cheng, H., Ling, Z., Louie, P., and Ayoko, G.: Which emission sources are responsible for the volatile organic compounds in the atmosphere of Pearl River Delta?, Journal of Hazardous Materials, 188, 116-124, https://doi.org/10.1016/j.jhazmat.2011.01.081, 2011.
Guo, H., Ling, Z., Cheng, H., Simpson, I., Lyu, X., Wang, X., Shao, M., Lu, H., Ayoko, G., and Zhang, Y.: Tropospheric volatile organic compounds in China, Science of The Total Environment, 574, 1021-1043, https://doi.org/10.1016/j.scitotenv.2016.09.116, 2017.
Han, Y., Wang, T., Li, R., Fu, H., Duan, Y., Gao, S., Zhang, L., and Chen, J.: Measurement report: Volatile organic compound characteristics of the different land-use types in Shanghai: spatiotemporal variation, source apportionment and impact on secondary formations of ozone and aerosol, Atmospheric Chemistry and Physics, 23, 2877-2900, https://doi.org/10.5194/acp-23-2877-2023, 2023.
Henry, R. F.: Weekday/weekend differences in gasoline related hydrocarbons at coastal PAMS sites due to recreational boating, Atmospheric Environment, 75, 58-65, https://doi.org/10.1016/j.atmosenv.2013.03.053, 2013.
Hsieh, H.-C., Ou-Yang, C.-F., and Wang, J.-L.: Revelation of coupling biogenic with anthropogenic isoprene by highly time-resolved observations, Aerosol Air Quality Research, 17, 721-729, https://doi.org/10.4209/aaqr.2016.04.0133, 2017.

908 Huang, Y. S. and Hsieh, C. C.: Ambient volatile organic compound presence in the highly urbanized city:
909 source apportionment and emission position, Atmospheric Environment, 206, 45-59,
910 https://doi.org/10.1016/j.atmosenv.2019.02.046, 2019.
911 Hui, L., Liu, X., Tan, Q., Feng, M., An, J., Qu, Y., Zhang, Y., and Jiang, M.: Characteristics, source
912 apportionment and contribution of VOCs to ozone formation in Wuhan, Central China, Atmospheric
913 Environment, 192, 55-71, https://doi.org/10.1016/j.atmosenv.2018.08.042, 2018.
914 Jung, U. and Choi, S.-S.: Variation in abundance ratio of isoprene and dipentene produced from wear
915 particles composed of natural rubber by pyrolysis depending on the particle size and thermal aging,
916 Polymers, 15, 929, https://doi.org/10.3390/polym15040929, 2023.
917 Kim, E., Brown, S. G., Hafner, H. R., and Hopke, P. K.: Characterization of non-methane volatile organic
918 compounds sources in Houston during 2001 using positive matrix factorization, Atmospheric
919 Environment, 39, 5934-5946, https://doi.org/10.1016/j.atmosenv.2005.06.045, 2005.
920 Kleinman, L. I., Daum, P. H., Lee, Y. N., Nunnermacker, L. J., Springston, S. R., Weinstein-Lloyd, J.,
921 and Rudolph, J.: Ozone production efficiency in an urban area, Journal of Geophysical Research:
922 Atmospheres, 107, ACH 23-21-ACH 23-12, https://doi.org/10.1029/2002JD002529, 2002.
923 Ko, Y.-C.: Air Pollution and Its Health Effects on Residents in Taiwanese Communities, The Kaohsiung
924 Journal of Medical Sciences, 12, 657-699, https://doi.org/10.6452/kjms.199612.0657, 1996.
925 Kumar, A., Sinha, V., Shabin, M., Hakkim, H., Bonsang, B., and Gros, V.: Non-methane hydrocarbon
926 (NMHC) fingerprints of major urban and agricultural emission sources for use in source apportionment
927 studies, Atmospheric Chemistry Physics, 20, 12133-12152, 2020.
928 Kuo, C.-P., Liao, H.-T., Chou, C. C.-K., and Wu, C.-F.: Source apportionment of particulate matter and
929 selected volatile organic compounds with multiple time resolution data, Science of the Total Environment,
930 472, 880-887, 2014.
931 Languille, B., Gros, V., Petit, J.-E., Honoré, C., Baudic, A., Perrussel, O., Foret, G., Michoud, V., Truong,
932 F., and Bonnaire, N.: Wood burning: A major source of Volatile Organic Compounds during wintertime
933 in the Paris region, Science of The Total Environment, 711, 135055,
934 https://doi.org/10.1016/j.scitotenv.2019.135055, 2020.
935 Lau, A. K. H., Yuan, Z., Yu, J. Z., and Louie, P. K.: Source apportionment of ambient volatile organic
936 compounds in Hong Kong, Science of the total environment, 408, 4138-4149,
937 https://doi.org/10.1016/j.scitotenv.2010.05.025, 2010.
938 Leuchner, M. and Rappenglück, B.: VOC source–receptor relationships in Houston during TexAQS-II,
939 Atmospheric Environment, 44, 4056-4067, https://doi.org/10.1016/j.atmosenv.2009.02.029, 2010.
940 Li, C., Liu, Y., Cheng, B., Zhang, Y., Liu, X., Qu, Y., An, J., Kong, L., Zhang, Y., and Zhang, C.: A
941 comprehensive investigation on volatile organic compounds (VOCs) in 2018 in Beijing, China:
942 Characteristics, sources and behaviours in response to O3 formation, Science of the Total Environment,
943 806, 150247, https://doi.org/10.1016/j.scitotenv.2021.150247, 2022.
944 Li, J., Xie, S., Zeng, L., Li, L., Li, Y., and Wu, R.: Characterization of ambient volatile organic
945 compounds and their sources in Beijing, before, during, and after Asia-Pacific Economic Cooperation

China 2014, Atmospheric Chemistry and Physics, 15, 7945-7959, https://doi.org/10.5194/acp-15-7945-2015, 2015.
Li, K., Jacob, D. J., Liao, H., Shen, L., Zhang, Q., and Bates, K. H.: Anthropogenic drivers of 2013–2017 trends in summer surface ozone in China, Proceedings of the National Academy of Sciences, 422-427,
Li, L. and Wang, X.: Seasonal and diurnal variations of atmospheric non-methane hydrocarbons in Guangzhou, China, Int J Environ Res Public Health, 9, 1859-1873, https://doi.org/10.3390/ijerph9051859, 2012.
Liao, H.-T., Yen, C.-M., Chen, Y.-R., Wu, J.-D., Tsai, S.-W., and Wu, C.-F.: Vertical variation of source-apportioned PM2. 5 and selected volatile organic compounds near an elevated expressway in an urban area, Environmental Science Pollution Research, 31, 20477-20487, 2024.
Liao, H.-T., Yau, Y.-C., Huang, C.-S., Chen, N., Chow, J. C., Watson, J. G., Tsai, S.-W., Chou, C. C.-K., and Wu, C.-F.: Source apportionment of urban air pollutants using constrained receptor models with a priori profile information, Environmental Pollution, 227, 323-333, 2017.
Lin, C.-W., Chiang, S.-B., and Lu, S.-J.: Investigation of MTBE and aromatic compound concentrations at a gas service station, Environmental Monitoring Assessment, 105, 327-339, 2005.
Lin, C.-Y., Wang, Z., Chou, C. C. K., Chang, C.-C., and Liu, S. C.: A numerical study of an autumn high ozone episode over southwestern Taiwan, Atmospheric Environment, 41, 3684-3701, https://doi.org/10.1016/j.atmosenv.2006.12.050, 2007.
Lingwall, J. W. and Christensen, W. F.: Pollution source apportionment using a priori information and positive matrix factorization, Chemometrics Intelligent Laboratory Systems, 87, 281-294, https://doi.org/10.1016/j.chemolab.2007.03.007, 2007.
Liu, Y., Shao, M., Fu, L., Lu, S., Zeng, L., and Tang, D.: Source profiles of volatile organic compounds (VOCs) measured in China: Part I, Atmospheric Environment, 42, 6247-6260, https://doi.org/10.1016/j.atmosenv.2008.01.070, 2008a.
Liu, Y., Shao, M., Lu, S., Chang, C.-C., Wang, J.-L., and Fu, L.: Source apportionment of ambient volatile organic compounds in the Pearl River Delta, China: Part II, Atmospheric Environment, 42, 6261-6274, https://doi.org/10.1016/j.atmosenv.2008.02.027, 2008b.
McFiggans, G., Mentel, T. F., Wildt, J., Pullinen, I., Kang, S., Kleist, E., Schmitt, S., Springer, M., Tillmann, R., and Wu, C.: Secondary organic aerosol reduced by mixture of atmospheric vapours, Nature, 565, 587-593, https://doi.org/10.1038/s41586-018-0871-y, 2019.
Mo, Z., Shao, M., Lu, S., Niu, H., Zhou, M., and Sun, J.: Characterization of non-methane hydrocarbons and their sources in an industrialized coastal city, Yangtze River Delta, China, Science of the Total Environment, 593, 641-653, https://doi.org/10.1016/j.scitotenv.2017.03.123, 2017.
Mo, Z., Shao, M., Lu, S., Qu, H., Zhou, M., Sun, J., and Gou, B.: Process-specific emission characteristics of volatile organic compounds (VOCs) from petrochemical facilities in the Yangtze River Delta, China, Science of the Total Environment, 533, 422-431, https://doi.org/10.1016/j.scitotenv.2015.06.089, 2015.
Implementation of Air Pollution Control Plan Achieves Remarkable Results, last access: 2025-12-04.
Latest Air Pollution Inventory Shows 19% Reduction Compared to Last Edition, last access: 2025-12-

04.
Na, K. and Kim, Y. P.: Chemical mass balance receptor model applied to ambient C2–C9 VOC concentration in Seoul, Korea: effect of chemical reaction losses, Atmospheric Environment, 41, 6715-6728, https://doi.org/10.1016/j.atmosenv.2007.04.054, 2007.
Nakashima, Y., Kamei, N., Kobayashi, S., and Kajii, Y.: Total OH reactivity and VOC analyses for gasoline vehicular exhaust with a chassis dynamometer, Atmospheric Environment, 44, 468-475, https://doi.org/10.1016/j.atmosenv.2009.11.006, 2010.
Nelson, P. and Quigley, S.: The hydrocarbon composition of exhaust emitted from gasoline fuelled vehicles, Atmospheric Environment, 18, 79-87, https://doi.org/10.1016/0004-6981(84)90230-0, 1984.
Nguyen, D. H., Hsieh, H. C., Chen, S. P., Ou-Yang, C. F., Chang, C. C., Liu, W. T., Wang, C. H., and Wang, J. L.: Analysis of high-ozone episodes using a chemical metric based on the reactivities of organic precursors, Journal of Geophysical Research: Atmospheres, 130, e2025JD043921, https://doi.org/10.1029/2025JD043921, 2025.
Paatero, P.: Least squares formulation of robust non-negative factor analysis, Chemometrics Intelligent Laboratory Systems, 37, 23-35, https://doi.org/10.1016/S0169-7439(96)00044-5, 1997.
Paatero, P. and Tapper, U.: Positive matrix factorization: A non-negative factor model with optimal utilization of error estimates of data values, Environmetrics, 5, 111-126, https://doi.org/10.1002/env.3170050203, 1994.
Pallavi, S. B. and Sinha, V.: Source apportionment of volatile organic compounds in the northwest Indo-Gangetic Plain using a positive matrix factorization model, Atmospheric Chemistry and Physics, 19, 15467-15482, https://doi.org/10.5194/acp-19-15467-2019, 2019.
Park, C., Schade, G. W., and Boedeker, I.: Characteristics of the flux of isoprene and its oxidation products in an urban area, Journal of Geophysical Research: Atmospheres, 116, https://doi.org/10.1029/2011JD015856, 2011.
Pedrozo, H. A., Reartes, S. B. R., Diaz, M. S., Vecchietti, A., and Grossmann, I. E.: Coproduction of ethylene and propylene based on ethane and propane feedstocks, in: Computer Aided Chemical Engineering, Elsevier, 907-912, https://doi.org/10.1016/B978-0-12-823377-1.50152-X, 2020.
Pekney, N. J., Davidson, C. I., Zhou, L., and Hopke, P. K.: Application of PSCF and CPF to PMF-modeled sources of PM2. 5 in Pittsburgh, Aerosol Science Technology, 40, 952-961, https://doi.org/10.1080/02786820500543324, 2006.
Peron, A., Graus, M., Striednig, M., Lamprecht, C., Wohlfahrt, G., and Karl, T.: Deciphering anthropogenic and biogenic contributions to selected non-methane volatile organic compound emissions in an urban area, Atmospheric Chemistry Physics, 24, 7063-7083, 2024.
Pollack, I., Ryerson, T., Trainer, M., Parrish, D., Andrews, A., Atlas, E. L., Blake, D., Brown, S., Commane, R., and Daube, B.: Airborne and ground-based observations of a weekend effect in ozone, precursors, and oxidation products in the California South Coast Air Basin, Journal of Geophysical Research: Atmospheres, 117, https://doi.org/10.1029/2011JD016772, 2012.
Ramírez, A. S., Ramondt, S., Van Bogart, K., and Perez-Zuniga, R.: Public awareness of air pollution

and health threats: challenges and opportunities for communication strategies to improve environmental health literacy, Journal of Health Communication, 24, 75-83, https://doi.org/10.1080/10810730.2019.1574320, 2019.

Ren, J. and Xie, S.: Diagnosing ozone-NOx-VOC sensitivity and revealing causes of ozone increases in China based on 2013–2021 satellite retrievals, Atmospheric Chemistry Physics Discussions, 2022, 1-22, https://doi.org/10.5194/acp-22-15035-2022, 2022.

Rubin, J. I., Kean, A. J., Harley, R. A., Millet, D. B., and Goldstein, A. H.: Temperature dependence of volatile organic compound evaporative emissions from motor vehicles, Journal of Geophysical Research: Atmospheres, 111, https://doi.org/10.1029/2005JD006458, 2006.

Scheff, P. A., Wadden, R. A., Bates, B. A., and Aronian, P. F.: Source fingerprints for receptor modeling of volatile organics, Japca, 39, 469-478, https://doi.org/10.1080/08940630.1989.10466546, 1989.

Shao, P., An, J., Xin, J., Wu, F., Wang, J., Ji, D., and Wang, Y.: Source apportionment of VOCs and the contribution to photochemical ozone formation during summer in the typical industrial area in the Yangtze River Delta, China, Atmospheric Research, 176, 64-74, https://doi.org/10.1016/j.atmosres.2016.02.015, 2016.

Shen, L., Xiang, P., Liang, S., Chen, W., Wang, M., Lu, S., and Wang, Z.: Sources profiles of volatile organic compounds (VOCs) measured in a typical industrial process in Wuhan, Central China, Atmosphere, 9, 297, https://doi.org/10.3390/atmos9080297, 2018.

Sillman, S.: The relation between ozone, NOx and hydrocarbons in urban and polluted rural environments, Atmospheric Environment, 33, 1821-1845, https://doi.org/10.1016/S1352-2310(98)00345-8, 1999.

Song, M., Tan, Q., Feng, M., Qu, Y., Liu, X., An, J., and Zhang, Y.: Source apportionment and secondary transformation of atmospheric nonmethane hydrocarbons in Chengdu, Southwest China, Journal of Geophysical Research: Atmospheres, 123, 9741-9763, https://doi.org/10.1029/2018JD028479, 2018.

Song, M., Li, X., Yang, S., Yu, X., Zhou, S., Yang, Y., Chen, S., Dong, H., Liao, K., and Chen, Q.: Spatiotemporal variation, sources, and secondary transformation potential of VOCs in Xi'an, China, Atmospheric Chemistry Physics Discussions, 2020, 1-34, https://doi.org/10.5194/acp-21-4939-2021, 2020.

Su, Y.-C., Chen, S.-P., Tong, Y.-H., Fan, C.-L., Chen, W.-H., Wang, J.-L., and Chang, J. S.: Assessment of regional influence from a petrochemical complex by modeling and fingerprint analysis of volatile organic compounds (VOCs), Atmospheric Environment, 141, 394-407, https://doi.org/10.1016/j.atmosenv.2016.07.006, 2016.

Su, Y. C., Chen, W. H., Fan, C. L., Tong, Y. H., Weng, T. H., Chen, S. P., Kuo, C. P., Wang, J. L., and Chang, J. S.: Source Apportionment of Volatile Organic Compounds (VOCs) by Positive Matrix Factorization (PMF) supported by Model Simulation and Source Markers - Using Petrochemical Emissions as a Showcase, Environmental Pollution, 254, 112848, https://doi.org/10.1016/j.envpol.2019.07.016, 2019.

Swarthout, R. F., Russo, R. S., Zhou, Y., Hart, A. H., and Sive, B. C.: Volatile organic compound

distributions during the NACHTT campaign at the Boulder Atmospheric Observatory: Influence of urban and natural gas sources, Journal of Geophysical Research: Atmospheres, 118, 10,614-610,637, 2013.

Thiruvenkataswamy, P., Eljack, F. T., Roy, N., Mannan, M. S., and El-Halwagi, M. M.: Safety and techno-economic analysis of ethylene technologies, Journal of Loss Prevention in the Process Industries, 39, 74-84, https://doi.org/10.1016/j.jlp.2015.11.019, 2016.

Thompson, C. R., Hueber, J., and Helmig, D.: Influence of oil and gas emissions on ambient atmospheric non-methane hydrocarbons in residential areas of Northeastern Colorado, Elementa, 3, 000035, 2014.

Vettikkat, L., Miettinen, P., Buchholz, A., Rantala, P., Yu, H., Schallhart, S., Petäjä, T., Seco, R., Männistö, E., and Kulmala, M.: High emission rates and strong temperature response make boreal wetlands a large source of isoprene and terpenes, Atmospheric Chemistry Physics, 23, 2683-2698, 2023.

Wang, C., Li, X., Miao, X., Li, J., Li, Y., Song, C., Yang, Z., Qi, J., and Jin, T.: Diesel vehicle emissions: Dissecting the multi-factorial effect on variations of VOC-component concentrations, Urban Climate, 58, 102157, https://doi.org/10.1016/j.uclim.2024.102157, 2024.

Wang, H., Lou, S., Huang, C., Qiao, L., Tang, X., Chen, C., Zeng, L., Wang, Q., Zhou, M., and Lu, S.: Source profiles of volatile organic compounds from biomass burning in Yangtze River Delta, China, Aerosol Air Quality Research, 14, 818-828, 2014.

Wang, Q., Li, S., Dong, M., Li, W., Gao, X., Ye, R., and Zhang, D.: VOCs emission characteristics and priority control analysis based on VOCs emission inventories and ozone formation potentials in Zhoushan, Atmospheric Environment, 182, 234-241, https://doi.org/10.1016/j.atmosenv.2018.03.034, 2018.

Wang, W., van der A, R., Ding, J., van Weele, M., and Cheng, T.: Spatial and temporal changes of the ozone sensitivity in China based on satellite and ground-based observations, Atmospheric Chemistry Physics, 21, 7253-7269, https://doi.org/10.5194/acp-21-7253-2021, 2021.

Wei, W., Lv, Z., Yang, G., Cheng, S., Li, Y., and Wang, L.: VOCs emission rate estimate for complicated industrial area source using an inverse-dispersion calculation method: A case study on a petroleum refinery in Northern China, Environmental Pollution, 218, 681-688, https://doi.org/10.1016/j.envpol.2016.07.062, 2016.

Wernis, R. A., Kreisberg, N. M., Weber, R. J., Drozd, G. T., and Goldstein, A. H.: Source apportionment of VOCs, IVOCs and SVOCs by positive matrix factorization in suburban Livermore, California, Atmospheric Chemistry and Physics, 22, 14987-15019, https://doi.org/10.5194/acp-22-14987-2022, 2022.

Wu, F., Yu, Y., Sun, J., Zhang, J., Wang, J., Tang, G., and Wang, Y.: Characteristics, source apportionment and reactivity of ambient volatile organic compounds at Dinghu Mountain in Guangdong Province, China, Science of the Total Environment, 548, 347-359, https://doi.org/10.1016/j.scitotenv.2015.11.069, 2016.

Wu, S., Alaimo, C. P., Green, P. G., Young, T. M., Zhao, Y., Liu, S., Kuwayama, T., and Kleeman, M. J.: Source apportionment of Volatile Organic Compounds (VOCs) in the South Coast Air Basin (SoCAB) During RECAP-CA, Atmospheric Environment, 338, 120847,

https://doi.org/10.1016/j.atmosenv.2024.120847, 2024.
Xie, Y. and Berkowitz, C. M.: The use of positive matrix factorization with conditional probability functions in air quality studies: an application to hydrocarbon emissions in Houston, Texas, Atmospheric Environment, 40, 3070-3091, https://doi.org/10.1016/j.atmosenv.2005.12.065, 2006.
Xu, H., Jia, Y., Sun, Z., Su, J., Liu, Q. S., Zhou, Q., and Jiang, G.: Environmental pollution, a hidden culprit for health issues, Eco-Environment Health, 1, 31-45, https://doi.org/10.1016/j.eehl.2022.04.003, 2022.
Xu, Z., Huang, X., Nie, W., Chi, X., Xu, Z., Zheng, L., Sun, P., and Ding, A.: Influence of synoptic condition and holiday effects on VOCs and ozone production in the Yangtze River Delta region, China, Atmospheric Environment, 168, 112-124, https://doi.org/10.1016/j.atmosenv.2017.08.035, 2017.
Yang, Y., Liu, B., Hua, J., Yang, T., Dai, Q., Wu, J., Feng, Y., and Hopke, P. K.: Global review of source apportionment of volatile organic compounds based on highly time-resolved data from 2015 to 2021, Environ Int, 165, 107330, https://doi.org/10.1016/j.envint.2022.107330, 2022.
Yeh, C.-K., Lin, C., Shen, H.-C., Cheruiyot, N. K., Nguyen, D.-H., and Chang, C.-C.: Real-time energy consumption and air pollution emission during the transpacific crossing of a container ship, Scientific Reports, 12, 15272, https://doi.org/10.1038/s41598-022-19605-7, 2022.
Zeng, J., Zhang, Y., Mu, Z., Pang, W., Zhang, H., Wu, Z., Song, W., and Wang, X.: Temperature and light dependency of isoprene and monoterpene emissions from tropical and subtropical trees: Field observations in south China, Applied Geochemistry, 155, 105727, 2023.
Zhang, K., Li, L., Huang, L., Wang, Y., Huo, J., Duan, Y., Wang, Y., and Fu, Q.: The impact of volatile organic compounds on ozone formation in the suburban area of Shanghai, Atmospheric Environment, 232, 117511, https://doi.org/10.1016/j.atmosenv.2020.117511, 2020.
Zhang, X., Han, L., Wei, H., Tan, X., Zhou, W., Li, W., and Qian, Y.: Linking urbanization and air quality together: A review and a perspective on the future sustainable urban development, Journal of Cleaner Production, 346, 130988, https://doi.org/10.1016/j.jclepro.2022.130988, 2022.
Zhang, Y., Li, R., Fu, H., Zhou, D., and Chen, J.: Observation and analysis of atmospheric volatile organic compounds in a typical petrochemical area in Yangtze River Delta, China, Journal of Environmental Sciences, 71, 233-248, https://doi.org/10.1016/j.jes.2018.05.027, 2018.
Zhang, Y., Wang, X., Zhang, Z., Lü, S., Huang, Z., and Li, L.: Sources of C2–C4 alkenes, the most important ozone nonmethane hydrocarbon precursors in the Pearl River Delta region, Science of the Total Environment, 502, 236-245, https://doi.org/10.1016/j.scitotenv.2014.09.024, 2015.
Zhou, S., Davy, P. K., Huang, M., Duan, J., Wang, X., Fan, Q., Chang, M., Liu, Y., Chen, W., and Xie, S.: High-resolution sampling and analysis of ambient particulate matter in the Pearl River Delta region of southern China: source apportionment and health risk implications, Atmospheric Chemistry and Physics, 18, 2049-2064, https://doi.org/10.5194/acp-18-2049-2018, 2018.
Zou, Y., Deng, X. J., Deng, T., Yin, C. Q., and Li, F.: One-year characterization and reactivity of isoprene and its impact on surface ozone formation at a suburban site in Guangzhou, China, Atmosphere, 10, 201, https://doi.org/10.3390/atmos10040201, 2019.

Zou, Y., Deng, X., Zhu, D., Gong, D., Wang, H., Li, F., Tan, H., Deng, T., Mai, B., and Liu, X.: Characteristics of 1 year of observational data of VOCs, NO x and O 3 at a suburban site in Guangzhou, China, Atmospheric Chemistry and Physics, 15, 6625-6636, https://doi.org/10.5194/acp-15-6625-2015, 2015.